

***REVISED: Milestone SP3B2BM4***  
**Report on CDP Reflection Image and Subsurface  
Structure Along Lines B and C: UZ-16 VSP**

**February 9, 1998**

WBS 1.2.3.11.2 Surface Geophysics

**M. A. Feighner, T. M. Daley, R. Gritto, and E. L. Majer**

*Earth Sciences Division  
Ernest Orlando Lawrence Berkeley National Laboratory  
Berkeley, California, 94720*

9903020115 990223  
PDR WASTE PDR  
WM-11  
/ /

**REVISED: Milestone SP3B2BM4**

**Report on CDP reflection image and subsurface structure along lines B and C: UZ-16 VSP**

**February 9, 1998**

WBS 1.2.3.11.2 Surface Geophysics

M. A. Feighner, T. M. Daley, R. Gritto, and E. L. Majer  
Earth Sciences Division  
Ernest Orlando Lawrence Berkeley National Laboratory  
Berkeley, California, 94720

## **1. Introduction**

In September 1995, a multicomponent, multioffset Vertical Seismic Profile (VSP) experiment was carried out by the Colorado School of Mines (CSM) under the direction of the United States Geologic Survey (USGS) at Yucca Mountain, Nevada. This VSP was designed and acquired in support of hydrologic studies at well UE-25 UZ-16. Unique and sophisticated analysis tools were developed at CSM specifically for application to the UZ-16 VSP data (Erdemir, 1997, Balch and Erdemir, 1996, Balch, et. al., 1996). In a separate effort in 1995, Lawrence Berkeley National Laboratory (LBNL) conducted numerous conventional surface and borehole seismic studies aimed at developing a geophysical model of Yucca Mountain. In 1996 LBNL completed a report on Synthesis of Borehole and Geophysical Studies at Yucca Mountain (Majer, et al, 1996). The Majer, et al (1996) report contained minimal information from the CSM UZ-16 VSP because the analysis was still in progress. In July of 1997, LBNL was tasked to summarize the current state of the UZ-16 VSP data set, and to apply conventional state-of-the-art VSP analysis to the available data. The goals of this conventional analysis are to detect and determine the extent of the reflecting horizons within the depth column of the well, the continuity of the geophysical/geomechanical properties of these horizons, and to relate the VSP to the previous surface reflection studies.

This report is a summary of LBNL's work between July and September 1997 as related to common depth point (CDP) reflection imaging and other analysis methods (plus a few pertinent results from the CSM analysis in Appendix A). In addition we present a cost/benefit discussion regarding potential further processing of the UZ-16 VSP data.

## **2. Data Status Including QA Status**

The raw field data were delivered to the Yucca Mountain Project in April 1996 as qualified (Q) data. The Technical Data Information Form (TDIF) #305387 was submitted and Data Tracking

Number (DTN) TMUE25UZ16(096.001) was assigned. The field observer's notes were also submitted in April 1996 as "Observer's Log and related attachments for UE-25 UZ-16 VSP Phase 1, September and October 1995", (88 pages). The accession number for this information is: MOL.19960708.0145 and this data is qualified with DTN: TMUE25UZ16(096.001).

LBNL has received a copy of the observer's notes and they appear adequate and sufficient for processing and analysis of the field data. The field data are divided into source lines named A, B, C, G, and NYRC. LBNL has not, at this time, requested or obtained a copy of the raw field data tapes from YMP Technical Information Center. LBNL has received a copy of the data which was processed and reformatted by CSM. This copy consists of source lines B and C. Source lines A, G and NYRC were, apparently, not processed by CSM. The data tapes received by LBNL from CSM were edited, stacked, sorted and reformatted (as discussed below). The editing and stacking processes are non-trivial and significant effort would be required to bring lines A, G and NYRC to the same state as lines B and C. The data for lines B and C now consist of the 5 source orientations (a vertical force generating P waves and 4 angled force directions which can be combined to generate S-waves) for each source location, and 3 orthogonal receiver components for each sensor depth. The eight source shots have been edited and stacked and the three recording system data sets have been merged and sorted into the 96 sensor depths. In addition the CSM processed data have been converted to SEG-Y tape format and the following trace headers have values stored: shot, espnum, relev, rstatcn, rec\_dep, rec\_sloc, g\_level, geo\_comp, forc\_ang, sou\_sloc, gammax, gammay, gammaz, source, tilt\_ang. LBNL has not checked all these headers for accuracy nor for completeness and a summary description of the meaning of all the headers is not yet available although we assume it can be constructed from Erdemir (1997). Use of the header values simplifies further data analysis. In summary, all the raw data are qualified, lines B and C are in formats ready for further analysis, lines A, NYRC, and G are in raw format with effort necessary before any analysis could begin.

### 3. Data Acquisition

The UZ-16 VSP used 96 3-component seismic sensors (geophones) which were cemented into the borehole at 16 foot intervals between a pipe liner and the borehole wall. There were three OYO DAS-1 recording systems used to record all 288 channels (96 x 3) simultaneously. The seismic source was an OMNIPULSE Land Air Gun. Five orientations of the source were used at every source location. These orientations are a single vertical force, two force directions oriented under  $45^\circ$  with respect to the vertical perpendicular to the source receiver plane, and two force directions oriented under  $45^\circ$  with respect to the vertical in line with the source receiver plane. The data recorded using these source orientations can be combined to create equivalent P-wave and S-wave source data. Each source location data set is therefore the equivalent of a conventional 9-component VSP. For each of the original five source orientations, 8 shots of the OMNIPULSE were recorded. Five source lines were acquired with sources equally spaced along the line at 100 ft intervals (with some 50 ft intervals near the well). Line G was a short test line, lines A, B and C were the main data lines, and line NYRC (North Yucca Ridge Crest) was a line on the Yucca Mt. ridge road (Figure 1a). The total lengths of lines A, B, and C are 400 ft, 4400 ft, and 3000 ft,

respectively. Figure 1b) shows the locations of the VSP source lines. A total of over 120 source locations were used.

#### 4. Data Processing

The initial processing of the UZ-16 VSP data set consist of editing and stacking of the 8 source shots for each of the five sources. This is a time consuming process requiring expert judgement from the processor in deciding which of the eight shots to stack, and possibly using auto-editing routines from seismic processing software. After stacking, the data from the three recording systems need to be merged and sorted into a meaningful order (such as each of the five sources for each of the sensor depths, in depth order). At this point the vertical source and the vertical component sensor data can be analyzed with conventional VSP analysis tools. Use of the other source and receiver components would require additional stacking and component rotation.

The initial processing steps were completed by CSM for lines B and C. The data for Lines B and C was then reformatted to SEG-Y standard tapes (a geophysical industry standard) and transferred to LBNL. It is our understanding that this work was done with the software package ProMAX which is not qualified. However, this initial processing uses simple arithmetic algorithms (such as used in spread sheets) and therefore software qualification is not required under USGS QA program (Clay Hunter, personnel communication).

The SEG-Y tapes sent to LBNL from CSM have been read into the Focus v4.1 processing package. Focus is a geophysical industry standard processing analysis package with conventional state-of-the-art analysis tools. Focus v3.0 has been qualified within YMP and Focus v4.1 is in the process of being qualified by LBNL. Another geophysical industry processing package named SEISLINK v3.2 was used for more advanced processing as the results and limitations of FOCUS were not satisfactory. SEISLINK v3.2 also is in the process of being qualified by LBNL. The individual modules used from FOCUS and SEISLINK are discussed below.

Only the vertical source component for each shot is being processed. The other four components at each source location are in raw field data state and would need to be stacked to create orthogonally polarized S-wave sources. Similarly, only the vertical component geophone data are being processed. Use of the horizontal geophone components and the S-wave would require three component orientation and rotation beyond the scope of this report. However, we do note that the use by Erdemir (1997) of source and sensor rotation to maximize the amplitude and coherency of reflection events did provide a significant improvement in data quality (as discussed in Appendix A).

Inspection of the data from lines B and C shows a strong decrease in frequency content (notable past the 500 foot offset) and poor signal-to-noise ratio beyond 1500 feet (for the unrotated vertical component data, Figure 2). Initially, shots within 500 feet of the well were investigated in order to examine the continuity of the reflections away from the well. Sources away from the well have increasingly horizontal ray paths which limit the energy on the vertical component sensor. Our final analysis included sources within 900 feet of the well. Beyond this distance the reliable determination of the first arrival times of the incident wavefield was impossible using the vertical source and receiver components.

The processing conducted by LBNL began with the FOCUS package. A processing flow was developed that included the following Focus processors: AGC (trace balancing); STATIC (shifting the data once to align the down-going energy); FKFILTER (filter out the down-going energy); STATIC (shifting the data twice to 2-way time, so reflections are near horizontal); RUNMIX (spatial smoothing); and AGC.

The necessary separation of down-going (direct) and up-going (reflected) arrivals was a difficult process. Comparisons between F-K filtering (frequency-wavenumber domain) routines in FOCUS and Seislink were performed using various approaches and various filters. Additionally a median filtering (averaging aligned energy and subtracting the result) was tested. The analysis was complicated by the lack of coherent reflections. It was intended to preserve the lack of reflection coherency observed in the raw data while maximizing the signal-to-noise ratio of the reflection events. Certain processing algorithms can 'force' the reflection events to appear as laterally coherent energy from planer interfaces, and these algorithms can be appropriate in geologic regimes which match the assumptions, however, we do not believe the Yucca Mountain seismic response fits this model. Another complication in wavefield separation is the increasingly horizontal propagation with increasing source offset. At far offsets the apparent angle seen in a VSP between up-going and down-going events is smaller than at near offsets. Figure 3 shows the change in the apparent angle between 0 ft and 900 ft offset. This decrease in angle makes the separation more difficult, as the median filter depends on different move out between the down- and up-going waves. After various filtering schemes were attempted (as discussed in Appendix B), our final results used median filtering and preserved much of the incoherent nature of the reflections while enhancing the reflection strength enough to allow CDP mapping.

Figure 4 shows the filtered up-going data for source locations B0 to B900 (line B), while the filtered up-going data for source locations B0 to C900 (line C) are presented in Figure 5. These sections can be compared for overall frequency content, reflection coherency, but not for event alignment since each source location has a unique time vs depth reflectivity profile.

The next major step in processing is the VSP/CDP mapping. This is a projection of the reflection events from recorded time to depth-offset location using ray paths traced through a velocity model. The generation of the velocity model is a crucial step. A model of dipping layers as described by the YMP geologic model (Clayton *et al.*, 1997) was used with constant seismic velocities. The present velocity model includes a 6° east dip. This dip taken from the geologic model was independently estimated by Erdemir (1997). Furthermore, a model dip of 12° was tested, as discussed in appendix B. The velocities within the dipping horizons were adjusted to best match the observed travel times. A single velocity model could not match travel times from all source offsets. The velocity variation observed for the different source locations is shown in Figure 6. It is notable that source locations west of B200 have a slower velocity, especially in the lithophysal section of the Topopah unit. We believe this is an indication of lateral velocity variation. While modeling of lateral velocity variation is not within the scope of this study, it would (along with lateral attenuation variation) explain much of the apparent incoherence of reflective energy.

Once a velocity model is created, a seismic ray path connecting any source-receiver pair can be calculated. The calculation of ray paths also allows us to see the limits of imaging coverage by calculating the subsurface reflection point for each reflecting horizon and for each source-receiver pair. We used two commercial ray tracing programs, the Seislink package and the GX-II package. Example ray paths from GX-II are shown in Figure 7. Figure 7 also shows the length of the

selected reflecting interface being imaged. We observe that the geologic dip has a large effect on the subsurface coverage. The line C data are highly limited in their coverage because the reflection points are all up-dip, near the well. This effect is more pronounced for the deeper horizons. The line B data however have extended coverage (compared to a horizontal layer model). The velocity structure also affects the horizontal coverage because of refraction at interfaces.

After calculating ray paths, the reflected energy (from the median filtered data) is projected from its arrival time to the ray path reflection points corresponding to that arrival time. Each data time step has a unique reflection point and depth-offset location. The up-going seismic trace is 'stretched' to overlay the calculated reflection points. This projected data is then 'binned' into CDP traces to remove the variable 'stretching' seen after projection. The binned data is considered the final VSP-CDP section.

The VSP-CDP sections for line B and C are given in Figure 8 and 9, respectively. The geologic horizons (using a 6° dip) are shown as solid lines on the CDP sections. These sections are all depth-offset sections at 1:1 scale, allowing direct comparison of reflectivity for each source location.

The final processing flows used the following modules: In Focus - GIN (Input SEG-Y data from CSM); TRACKER ANALYZE (arrival time picker), HEADPUT (add header information including shot/receiver geometry and first arrival time picks); AGC (automatic gain control with 500 ms window ); GOUT (output SEG-Y data for input to SEISLINK). The processing then continued in SEISLINK with the following modules: SEG-Y INPUT (data input from FOCUS); Bandpass Filter (a 10 to 70 Hz filter); Median Filter (align down-going waves using first arrivals, apply 11 trace median filter, subtract from input data and output subtracted data representing the reflected energy); Median FILTER ( input the reflected energy and align up-going arrivals using a 5 trace median filter to enhance reflected energy); VSP-CDP TRANSFORM (perform velocity modeling to fit the observed arrivals; fit was within +/- 2 ms with errors up to +/- 5 ms for longer offsets; use a 10 foot square bin size for CDP mapping).

## 5. Interpretation

The interpretation of the VSP data is influenced by any variation of medium properties over the lateral extent the survey area. The underlying assumptions are a constant 6° east dip of the layers and a horizontally uniform velocity model. It is obvious that these assumptions constrain the reliability of the interpretation below. Figures 2a) and 2b) show an example of the amplitudes and spectral content of the raw data and the reflected energy, respectively. Three offsets along line B at distances of 0 ft (B0), 500 ft (B500), and 900 ft (B900) from the observation well, are chosen to indicate the change in frequency content over the length of the survey line. The spectral plots (at the bottom of the figures) represent the average of the spectra of the 96 traces above. It is apparent from Figure 2a that the relative frequency content drops with increasing offset. The frequency dependent loss in energy can be attributed to anelastic attenuation, while the local peaks and troughs may be caused by scattering processes. Whereas at zero offset the amplitude spectrum reveals nearly equal values above -25 dB between 40 Hz and 80 Hz, this level drops for the two offset locations particularly in the 40 Hz to 80 Hz band. However, the signal to noise ratio is still

acceptable with a noise level below -70 dB. The amplitude loss in the 0 Hz to 40 Hz band is less than at higher frequencies, revealing an almost uniform amplitude level for the 500 ft offset, and an unusual increase between 20 Hz and 30 Hz for the 900 ft relative to the 500 ft offset. This increase may be caused by multipathing and interference effects, increasing the amplitude level at the frequencies, or by near surface attenuation variation between source locations. A partial loss in frequency content is caused by propagation of the direct waves through the lithophysal zone which is highly attenuating (Kaelin and Johnson, 1997). The farther the offset, the longer the travel path of the incident waves in this zone, and consequently the higher the attenuation. Additionally, reduction of the amplitudes for the two far offsets in the shallow part of the well is caused by an increase in horizontal propagation of the rays in the medium. These horizontal rays produce small amplitudes on the analyzed vertical components in the upper part of the well.

A sample of the reflected waveforms is presented in Figure 2b. The overall trend mimics that of the incident wave. However, the two major differences are that the time sections are transformed into two way travel times, intended to flatten the reflecting horizons and help in the visual interpretation of the reflection events, and that the displayed frequency spectra are each individually normalized to their peak amplitudes. The seismogram sections reveal a decrease in high frequency energy with increasing offset. Additionally, high frequency scattered energy is apparent in the zero offset section between the coherent reflections and is increasingly attenuated in the two far offset sections. This attenuation is caused by the anelastic attenuation in the medium, and is more effective the longer the travel distance of the scattered phases. The limited lateral extension of the reflection points for the zero offset geometry (see Figure 7) reduces the number of traces which show coherent reflected energy. The extent of the reflective coherency increased for the 500 ft offset while it decreased for the far offset again. The change in slope of the events visible at later times in the far offset section, may be remnants of down going energy generated by multiple reflections along the propagation path of the direct wave, which was not properly removed by the median filter, as they reveal a different moveout than the direct incident waves.

The median filtered up-going wavefields for the offset along line B (0 ft to 900 ft) are presented in Figure 4. The purpose of this figure is to identify reflections visible in the time section that may eventually collapse into small spacial bins during the CDP mapping process. This is particularly important for reflections off interfaces mapped at the short offsets, as their lateral extent is short in the CDP maps. As mentioned above, the reflections in the time sections are not directly comparable from panel to panel as their total two way travel times change with changing offset distance. Therefore, the identification of the reflections will be done in one single offset panel while the lateral continuity will be investigated based on the CDP maps in Figure 8.

As indicated in offset B0 (Figure 4a) the identified reflections are associated with the following geological sections in depth order:

1. Base of Tiva / Top of Topopah zone (Tiva)/(Tptm)
2. Upper vitrophyre zone (Tptr1)
3. Topopah, upper lithophysal zone (Ttpul)
4. Topopah lower lithophysal zone (Ttpll)
5. Topopah lower nonlithophysal zone (Ttplt)
6. Top of Calico (Calico)
7. Reflections inside Prow Pass (Prow Pass)

The composition of the time sections reveals a drop in high frequency energy with increasing offset as pointed out in Figure 2. However, it can be observed that the reflections in offset B300 and B400 reveal the lowest frequency content of all offsets. A possible explanation will be given below. With increasing offset the coverage of the reflection points is decreased in the shallow subsurface (see Figure 7), and thus they can only be used to verify deeper reflections indicated in the zero offset map. The most prominent reflection in all of line B is the Prow Pass reflection which can be seen throughout the 700 ft offset. The zero offset section in Figure 8a) shows the collapse of the reflected amplitudes as seen in Figure 4a). The arrows indicate the location of the mapped horizons as listed above. Although the number of bins for this geometry is limited, the information is reliable as it is supported by the reflection points of many rays (see Figure 7). The lateral extent of the reflections can be estimated from the offset sequence in Figure 8.

The second and third offset (100 ft and 200 ft) support the findings of the zero offset section within the depth range of the well. The 300 ft and 400 ft offset maps, for the first time, offer larger reflection intervals and thus the possibility to reliably estimate the continuity of the reflectors within this limit. However, it becomes apparent that the reflections seem discontinuous with vertical shifts in their location. This is most apparent in the Calico sequence at 400 ft offset where reflections seem shifted by one half cycle of the wavelet, and also in the Prow Pass formation (see arrows). Furthermore it can be seen that there is a scattered appearance of reflective energy throughout the CDP map. This information in conjunction with the low frequency content visible in Figure 4 for the same offsets suggests the presence of a fault embedded in a fractured zone. A fractured zone constitutes a highly irregular medium for high frequency waves as they are scattered multiple times without lateral coherency of their reflections. The 500 ft offset map supports these findings. A shift of one half wavelength is visible throughout the lower Topopah and Calico formation, indicating the presence of a fault at an offset approximately 250 ft west of UZ-16. However, the internal Prow Pass reflections do not show any sizable disruptions. At greater depth, reflections become visible in the Bull Frog and Tram formations which indicate vertical disruptions as well. Although for geometric reasons, the ray coverage and actual mapping of the reflection amplitudes becomes less accurate with depth, the throw in the Tram formation might indicate that the same fault is present at this depth level. The last three processed offsets along line B (700 ft, 800 ft, and 900 ft) show the same incoherent reflected energy produced by scattering of the incident wave throughout the fault/fracture zone. The overall drop in frequency content is caused by continuous anelastic attenuation throughout the long propagation paths from the offsets to the well. Coherent reflective energy can possibly be associated with the lower Prow Pass section and the transition to the Bull Frog formation.

Because of the possibility of a fault fracture zone about 250 ft west of UZ-16, it is unlikely that the identified horizons are continuous across this feature given the possible throw as indicated in the CDP maps. However, based on the poor quality of the data from offsets west of the postulated fault zone, it is not possible to state whether the horizons regain their continuity which they appear to reveal east of the fault.

Figure 5 finally shows the time sections of the up-going wavefield for the C line from zero to 900 ft offset. Unfortunately, because of the east dipping interfaces, the coverage of this line is much more limited than for line B. The comparison of the far offset for line B and line C (see Figure 7) reveals the difference in lateral extent of the reflectors in the subsurface. Whereas the theoretical coverage of line B reaches out to 800 ft (for the deepest reflector) this limit is only 400

ft for line C (for a reflector at intermediate depth).

It should be noted that for the first offset (100 ft) the bounce points of the reflected waves almost coincide with those of the 100 ft offset of line B. Therefore, the character of reflections is very similar to their counterparts of line B and the same horizons can be identified in this section. It can be seen in Figure 5 that the frequency content is more gradually decreasing throughout the different offsets. However, referring to the CDP map of line C, as presented in Figure 9, it becomes apparent that the coverage of each reflection event is indeed poor and no reliable conclusions should be drawn from these results. In the shallow subsurface, however, the offset maps at 200 ft and 300 ft reveal reflections off the top of the Topopah zone indicating the extent of this feature out to a distance of at least 50 ft east of UZ-16. The farthest offsets (800 ft and 900 ft) reveal the same internal reflection within the Prow Pass formation as found along line B. Although the reflections appear to be undulating, they do not show any discontinuity up to their coverage limit at 150 ft east of UZ-16.

Figure 1b) shows the possibility of 3 faults crossing line C at around 300 ft, 350 ft, and 600 ft offset. However as indicated above, the reflections along line C do not extend far enough east of UZ-16 to investigate the existence of these faults at depth. Furthermore, the existing coverage is so poor that even within this range no reliable interpretation about possible disturbances of the detected horizons is possible.

## 6. Conclusions

The present study of VSP data at UZ-16 produced the following results: The quality of the recorded data is such that reflection imaging beyond an offset source distance of 900 ft. using present capabilities is unfeasible. A constant velocity model with a suggested dip of  $6^\circ$  east can best satisfy the arrival times of the recorded data. The maximum velocity variations between the furthest investigated offsets B900 and C900 is approximately 36 %, indicating lateral variation in the physical parameters of the medium properties. The available imaging software is limited to dipping but laterally constant velocity model, such that the lateral variation can only be taken into account in between different source positions, not within a single source gather. However, the overall continuity of the reflections from source to source offset indicates that the variations in the velocity model seem representative of the true variability.

Reflecting horizons could be identified within the depth range of UZ-16. Their lateral continuity towards the west is limited by the possible presence of a fault/fracture zone at approximately 250 ft. west of the well. The data indicates a throw of about 75-100 ft., although this estimate is the least confined result. It cannot be determined whether the throw is continuous throughout the imaged depth range, but seems to be extending from the Topopah lower lithophysal zone to the Calico formation. The correlation with the geologic units is possible with the VSP method because the data are actually recorded at the different geologic units and thus the reflector can be directly related to the core and log data from surface to the well bottom. While there is a surface mapped fault trace near this location, information about the mapped offset is not currently available.

The mapping along line C is very limited, caused by the east dipping layers. No information

can be extracted for the area east of UZ-16 down to the bottom of the well. The only reflections appear within the Prow Pass formation and are visible up to 200 ft. east of the well.

Deeper reflections are present in the data but without confirmation or ties to other data (P-1 VSP, Line 3 regional) it is not certain if these reflections could be the Paleozoic interface.

## **7. Cost Benefit Discussion of Future Work**

In this section we evaluate the potential of the current data set for the possibility of future work and list the costs associated with each individual task.

The VSP data recorded at UZ-16 represent a high quality seismic experiment. However, the heterogeneous, laterally varying nature of the material properties at Yucca Mountain, along with the maximum depth of UZ-16 sensors (1640 ft.) limit the results which could be obtained with conventional analysis. Our study indicates any lateral interpretation of reflections is limited to about 900 feet from the well. Other types of studies, such as velocity or attenuation tomography, which use direct (not reflected) arrivals, could have a larger radius of investigation. However, we believe useful results are probably limited to the immediate vicinity of the well. A study of imaging a fracture zone, for instance, would likely provide poor resolution (such as 100 ft. lateral and 200 ft. depth accuracy). Within 1000 feet of UZ-16, the VSP data does provide an example of the applicability of seismic imaging to Yucca Mountain. Since the VSP experiment used grouted 3-component geophones, it provides an example of "best case" seismic imaging. As such, there is significance to groups interested in predicting and monitoring the mechanical properties of the subsurface, such as tunnel boring engineers and earthquake hazard modelers. In particular, we believe the lateral variation in material properties is still underestimated within the project. Studying lateral variations within 1000 feet of UZ-16 could be seen as a study investigating the fundamental nature of faulting and fracturing at Yucca Mt as a function of depth, which would have future application to siting and monitoring the potential repository.

One limitation in the present study is the horizontally uniform velocity model which poses the constraint that the reflection point is assumed to lie in a vertical plane spanned by the source, the reflection point, and the receiver. However, lateral heterogeneity would cause the reflection point to move out of this plane. A joint rotation of source and receiver components to maximize the energy of all reflection events in the traces may reveal the true location of the reflector and shed light on the true heterogeneity of the medium. Our understanding of the lateral heterogeneity is probably already greater than that which is incorporated into hydrologic and seismic design models. However, when a potential repository site is accepted, more detailed analysis of material property heterogeneity may be necessary, and the UZ-16 study could then become a very useful analog and design tool for seismic studies.

We believe future work with the UZ-16 VSP data set should include a detailed investigation of the additional source/receiver components not utilized in the present study. This work should include shear-wave studies. The source components applied under various source angles can be combined to create horizontally and vertically polarized shear waves which are particularly suited to study the physics of fractured zones. The recorded shear waves would be investigated in terms of travel times and shear wave splitting to model fracture density and orientation. This study would

use direct arrivals and therefor could extend somewhat beyond the 1000 ft. radius along lines B and C. (Initial processing of Line A would be significant extra effort which is probably not justified at present). The actual radius of useful investigation can not be predetermined, however it is very unlikely that useful information would extend to the entire acquired offset (over 4000 ft.). An example result would be defining mapped surface faults as being (or not being) significant sub-surface fracture zones. Such information about the fracture zones could be useful to geologic and hydrologic flow modelers, however the VSP geometry provides limitations to the resolution attainable. The resolution would have trade-offs between variables such as fracture density and thickness of the fracture zone. We believe this project is worth undertaking because of the basic science and potential benefits to future seismic imaging studies.

Orientation of fracturing within a fracture zone can be estimated from shear-wave polarizations, and this information could be used in structural or tectonic models, however estimating this property at UZ-16 is probably not critical to the project. While the immediate vicinity of UZ-16 may not be critical, the expertise could be transferred to future sites which may need imaging of potential fracture zones.

Finally the data set may be investigated to determine the presence of deep reflections indicating the location and depth of the basement. This project would be hampered by the limited depth of the UZ-16 sensors, since the variable reflectivity makes identification of reflectors below the well difficult. However, the recently completed VSP at well P-1 would help basement interpretation. If a basement reflection was successfully interpreted, the result would contribute to the tectonic and structural model of Yucca Mountain and vicinity. While success is not guaranteed, this project seems worth undertaking.

The costs of these processing and interpretation steps are as follows:

#### Initial Processing:

Grouping and combining the data into single force-single receiver traces (i.e. P-wave and 2 S-waves) for each offset along line B and C (2 man-weeks, \$ 7,500.00).

#### Direct Arrival Studies:

Rotating the data to maximize energy for P- and S-waves, and estimating heterogeneity from rotation angles (1 man-month, \$ 15,000.00).

Modeling P- and S-wave propagation through various zones of fracture density and orientation using variable velocity and attenuation (2 man-months, \$ 30,000.00).

#### Reflection Studies:

Deconvolving the data set by the source waveforms and mapping the deeper reflections to image possible basement locations (3 man-months, \$ 45,000.00).

## 8. Appendix A

The following is a summary of the data processing and results obtained by CSM as reported in Erdemir, 1997. The investigations by CSM were aimed at imaging the subsurface in the vicinity of UZ-16.

The data processing is event oriented in that each sequence of processing flows is aimed at enhancing one single reflection. The processing consist of editing and stacking the traces, followed by a source and receiver component rotation to improve the signal to noise ratio. The travel times of the reflections associated with the event are taken as input for a two-eikonal migration routine (Reshef and Kosloff, 1986), This routine is intended to determine by trial and error a uniform velocity distribution and the correct event location by migrating the arrival times to numerous overlapping ellipses which, in the case of the right velocity, overlap to construct the correct reflector location. Applying this technique to a sequence of reflectors a 3 layered velocity model was determined. The velocity profile at the location of UZ-16 is as follows:

<u>Velocity [ft/s]</u>	<u>Depth [ft]</u>
8500	0 - 1700
9750	1700 - 3000
10500	> 3000

In addition a dip of  $6.25^\circ$  east is assumed for the layered model, estimated from the dip of a specific even associated with the Calico formation. Subsequent to the two-eikonal migration a reverse time migration is applied to the enhanced reflection amplitudes based on the predetermined velocity model described above. As before, the reverse time migration is an event oriented process enhancing a single reflector at a time, only.

The final results presented by CSM, are the velocity model as described above including a dip of  $6.25^\circ$ . Additionally two reflectors are determined at a depth of 1600 ft and 1700 ft. The first reflector is associated with the top of the Calico Hill formation, while the second images a reflection within the Prow Pass section.

The results as presented by CSM reveal similarities to the present study, in that we found a dip of  $6^\circ$  to provide the best fit between the CDP images and the geological model. Furthermore, the reflections from the Calico Hill and Prow Pass formation could be confirmed at the reported depth. However, the present study provides a more detailed image of the geology within the depth range of the borehole. Furthermore, it revealed considerable velocity variations across line B and C which, due to the chosen method, could not be found by CSM.

## 9. Appendix B

This section is intended to provide a brief summary of the analysis using a model of  $12^\circ$  east dipping constant velocity layers. The ray paths associated with this model for three offsets (B900),

B0, C900) are shown in Figure B1. This figure compares to Figure 7 for the model based on a 6° dip. Two effects of the steeper dip are visible. The first is a migration of the reflection points uphill, while the second is a shortening of the reflection points that cover the horizon at depth. Both effects will limit the possibility to study the extension of the horizons along line C. The ray tracing plot for the C900 offset reveals that the reflection points are very narrow in lateral extent for all depth ranges and limit the imaging to the western side of UZ-16 below the bottom of the well. Hence this model, assuming it provided the better fit, would be a severe limitation for the imaging of the eastern side of UZ-16 along line C.

Figure B2 shows the depth dependent velocity models that best fit the observed travel times for each offset (compare to Figure 6 above). It can be seen that for this model the velocity estimates tend to be low for the up-dip part of the model along line B while they show higher values for the down-dip part along line C. The comparison with Figure 6 shows that this discrepancy is less pronounced in the case of the 6° model.

The CDP maps for the 12° model are presented in Figures B3 (line B offsets) and B4 (line C offsets). It can be seen throughout the offsets of line B that the fit between the model horizons and the reflections is not good. The reflections within the depth interval of the borehole show steeper dips than assumed in the model in addition to incoherent amplitudes for further offsets. The deep reflections within the Prow Pass and Bull Frog formations show unrealistic horizontal undulations. Line C on the other hand shows the limitations in coverage as discussed above. The furthest extension of reflected energy reaches to about 100 ft west of UZ-16 at the bottom of the well.

Based on these results, we reject the 12° dip model as a representation of the geologic layering below along line B and C.

## 10. References

Balch, A. H. and C. Erdemir, A Nine-component, multiple-offset vertical seismic profile at the UE-25 UZ#16 Borehole, Nevada Test Site, Nye County, Nevada: Taking VSPs to a New Level, U.S. Geological Survey, YMP Branch/Foothills Engineering Co., Denver, Colorado, Milestone 3GUP622M, 1996, ACCN: Unavailable.

Balch, A. H., C. Erdemir, R. W. Spengler, and W. C. Hunter, Nine-Component, Vertical Seismic Profiling at Yucca Mountain, Nevada, U.S. Geologic Survey, Jan 16, 1996, ACCN: MOL.19961122.0433.

Clayton, R.W., Zelinski W.P., and Rautman C.A., 1997. ISM2.0: A 3D Geologic Framework and Integrated Site Model of Yucca Mountain, Report prepared by the Civilian Radioactive Waste Management System, Management and Operating Contractor to the U.S. Department of Energy, M&O Document Identifier B00000000-01717-5700-00004 Rev 00. Ascension No. MOL. 19970728.0283

Day, W. C., R. P. Dickerson, C. J. Potter, D. S. Sweetkind, C. A. San Juan, C. J. Fridrich, and R. Drake, 1997, Preliminary Geologic Map of Yucca Mountain Area, Bye County, Nevada, Not Review.

Erdemir, C., 1997, Interactive Polarization Filtering and Pre-Stack Imaging of Nine-Component, Multiple-Offset VSP Data, Yucca Mountain, Nevada, Ph.D. thesis, Colorado School of Mines, ACCN: Unavailable.

Kaelin B. and L. R. Johnson, 1997, Seismic rock properties of partially water saturated tuffs in the Yucca Mountain region derived from logs and VSP data, submitted to Geophysics, ACCN: Unavailable.

Majer, E. L., M. Feighner, L. Johnson, T. Daley, E. Karageorgi, K. H. Lee, K. Williams, and T. McEvelly, 1996, Synthesis of Borehole and Surface Geophysical Studies at Yucca Mountain, Nevada and Vicinity Volume I: Surface Geophysics, Yucca Mountain Project Milestone OB05M, Lawrence Berkeley National Laboratory, Berkeley, CA, 1996, DTN: LB960808314212.001 (Q), LB960808314212.002 (Q), LB960808314212.003 (Q), LB960808314212.004 (Q), ACCN: MOL.19970114.0137.

Reshef, M. and Kosloff, D., 1986, Migration of common shot gathers, Geophysics, V51, No. 2, pp. 324-331, ACCN: Unavailable.

## Table of Milestone Deliverables

<u>Deliverable Description</u>	<u>Report Section Containing Deliverable</u>
CDP reflection image and subsurface structure along each line	Section 4 and 5
Cost / Benefit discussion regarding further processing	Section 7

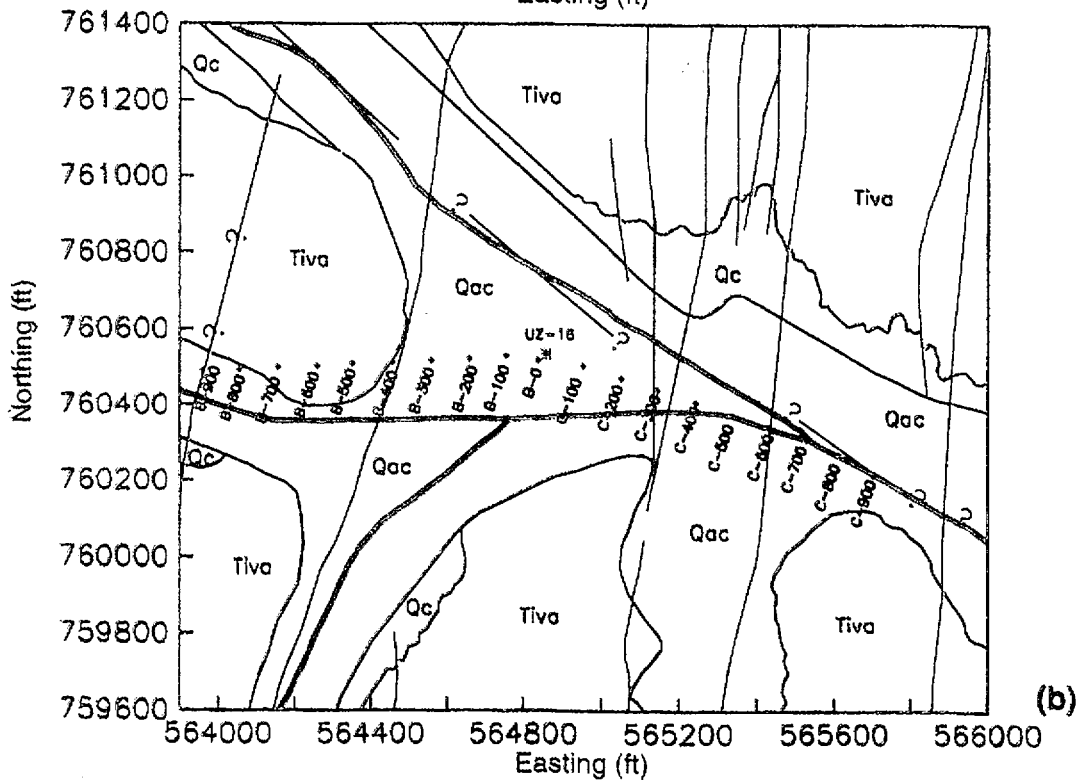
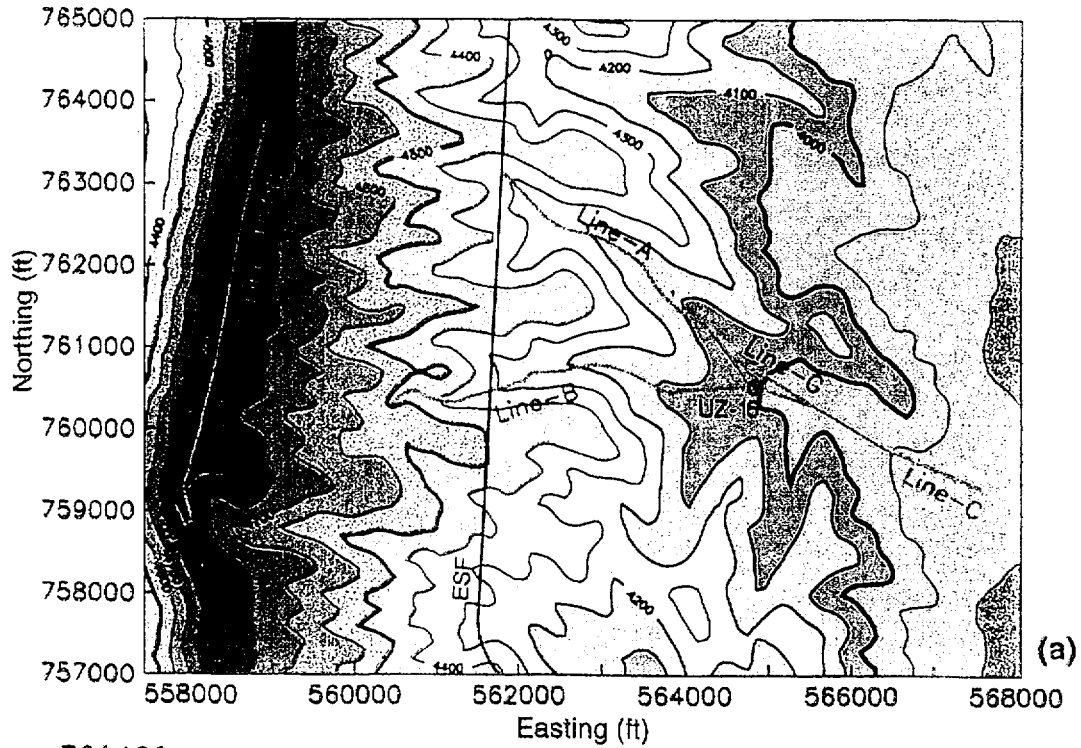


Figure 1. (a) Location of all the VSP lines shot with elevation contours; (b) Location of VSP shots for lines B and C within 900 feet of the UZ-16 well. Geologic data is from Day et al. (1997) and include: Faults (in red), Qac - alluvial and colluvial deposits; Qc - colluvial deposits; and Tiva - Tiva Canyon Tuff undivided. Roads are shown in blue.

## Frequency Content of Raw Data

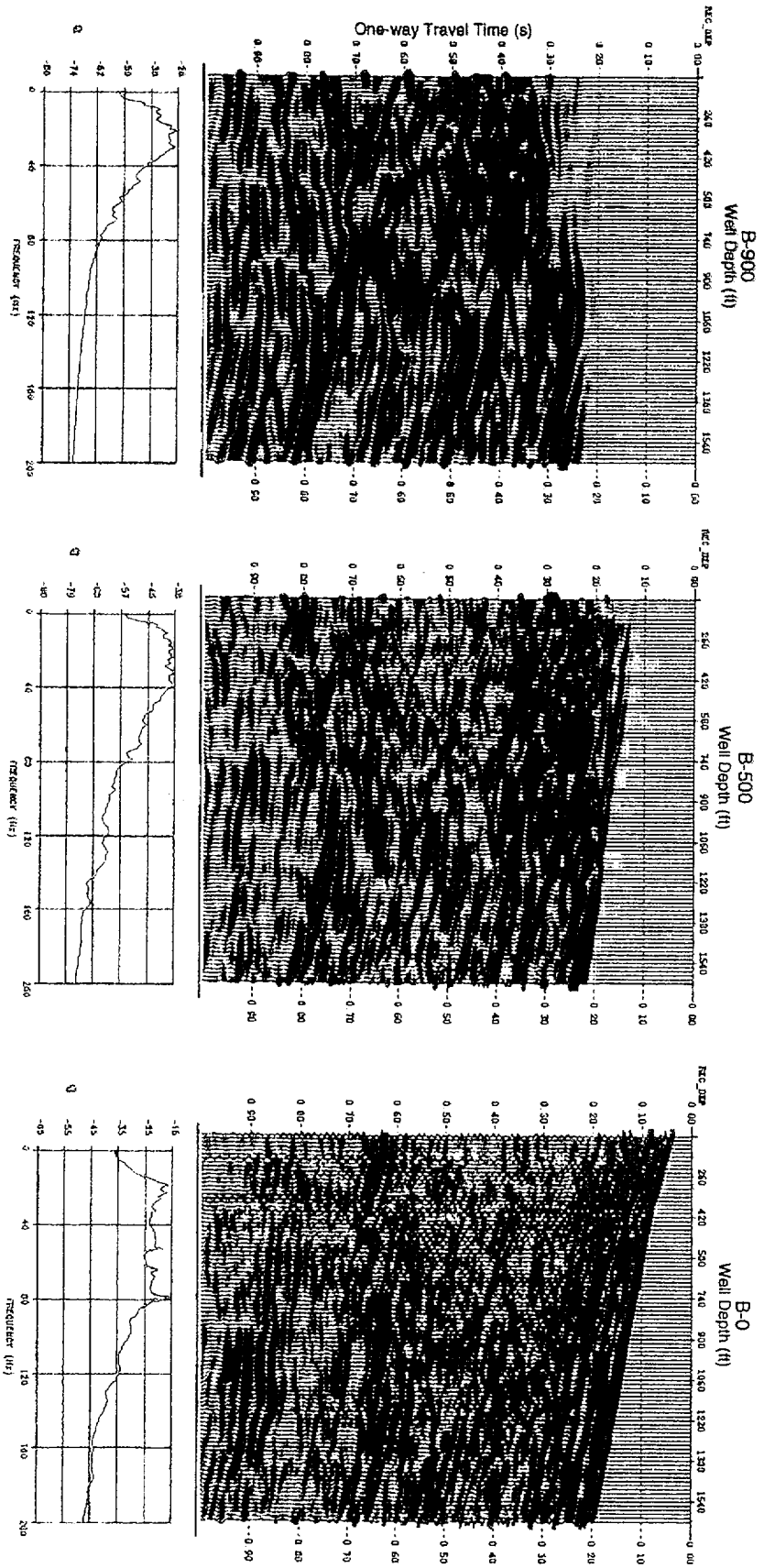


Figure 2a: Example of the raw data (top) and spectral content (bottom) for three offsets along line B.

# Frequency Content of Reflected Energy

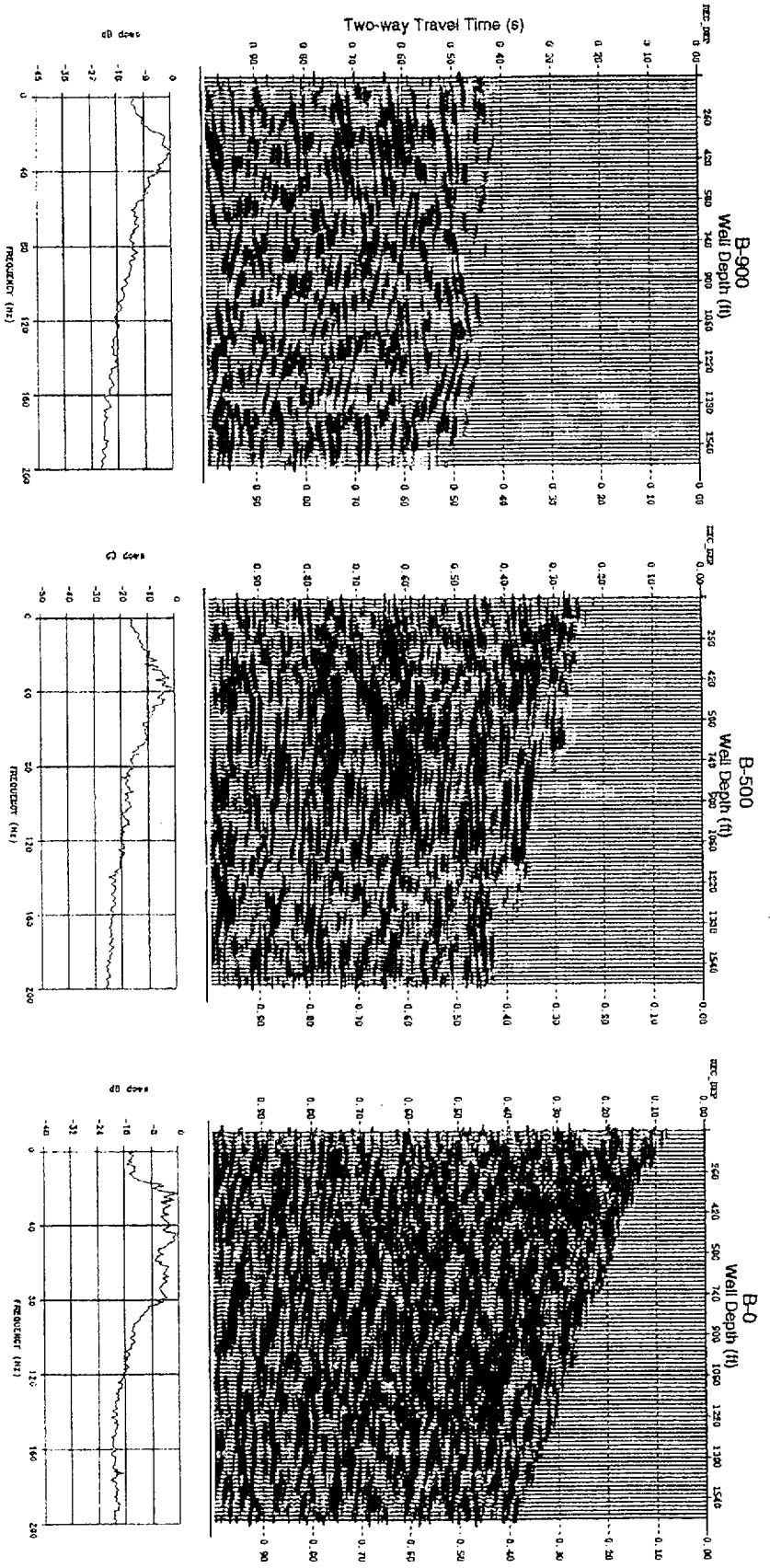


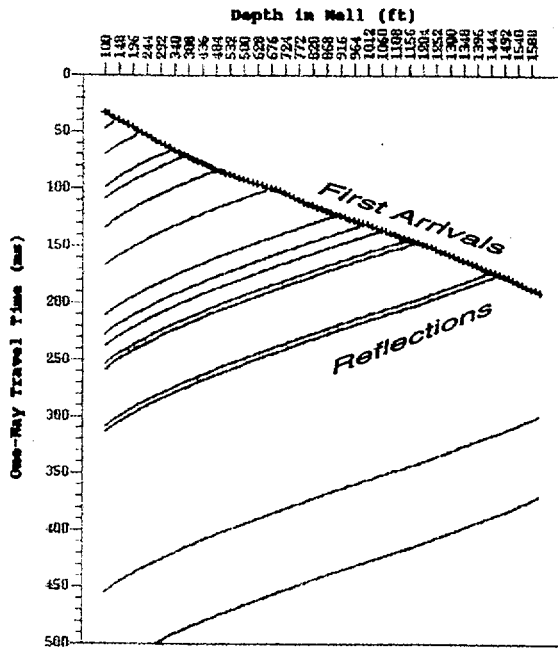
Figure 2b: Example of the reflection data (top) and spectral content (bottom) for three offsets along line B. The input for the reflection data is the raw data as presented in Figure 2a.

# Difficulty in Separating Downgoing & Upgoing Energy with Offset

a)

Model Response  
0-0

Zero Offset

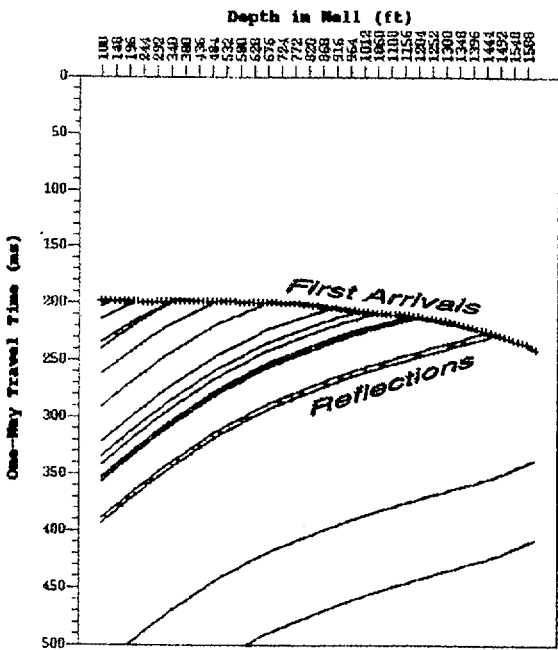


Large angle between first arrivals (down-going energy) and reflections (upgoing energy) at short offsets make wave separation easier.

b)

Model Response  
c-900

900 Foot Offset



Small angle between first arrivals (downgoing energy) and reflections (upgoing energy) at long offsets make wave separation difficult with standard processing flow.

Figure 3: Two examples revealing the different involute of the down- and upgoing waves: a) source at zero offset location b) source at 900 ft offset location

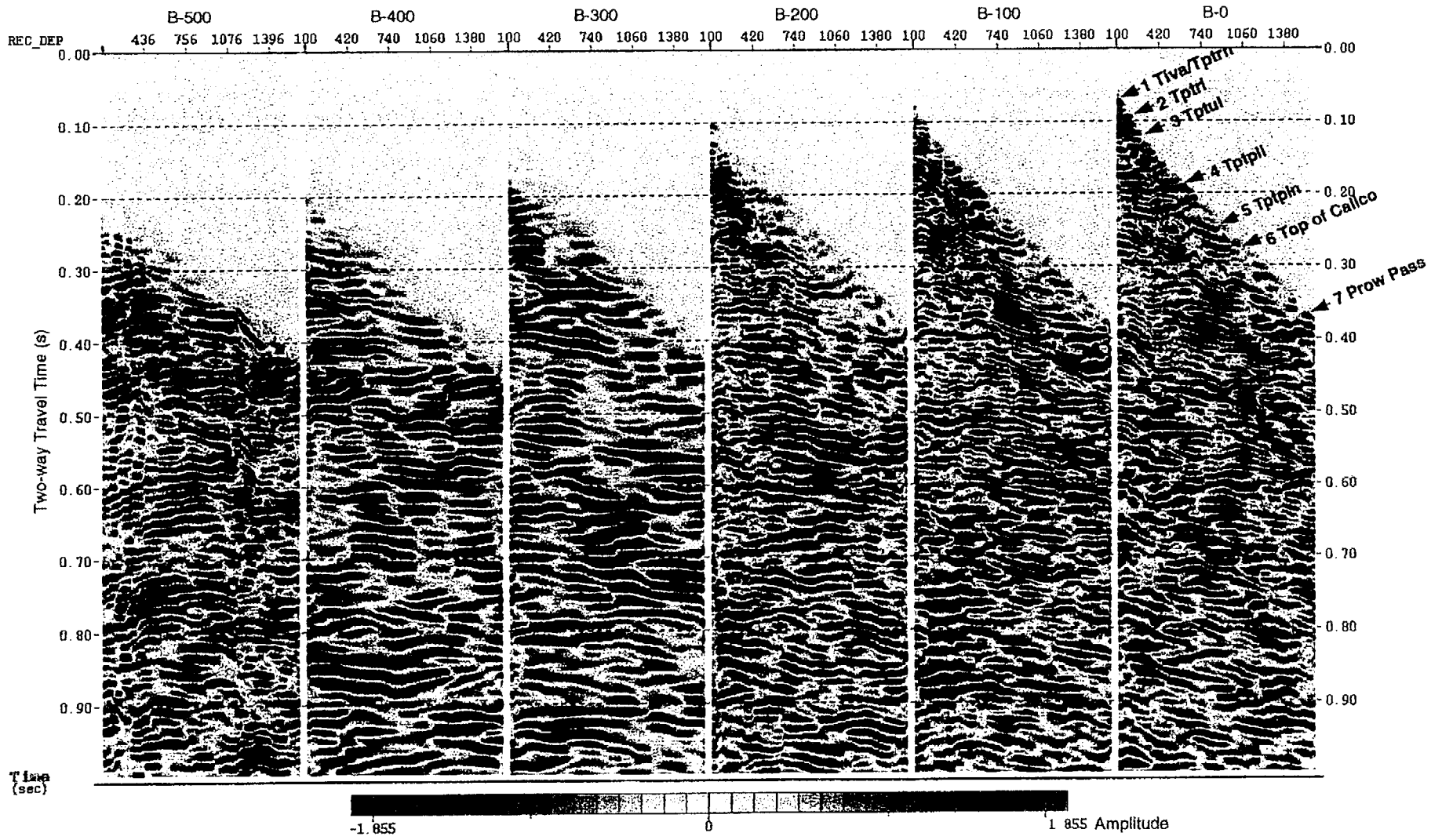


Figure 4a: Median filtered upgoing wavefield for source offsets of 0 ft - 500 ft. The data is time shifted by the two-way travel time to flatten the reflections and to help in the interpretation of the detected horizons. The identified events are indicated in the zero offset section (refer to the text for an explanation of the names).

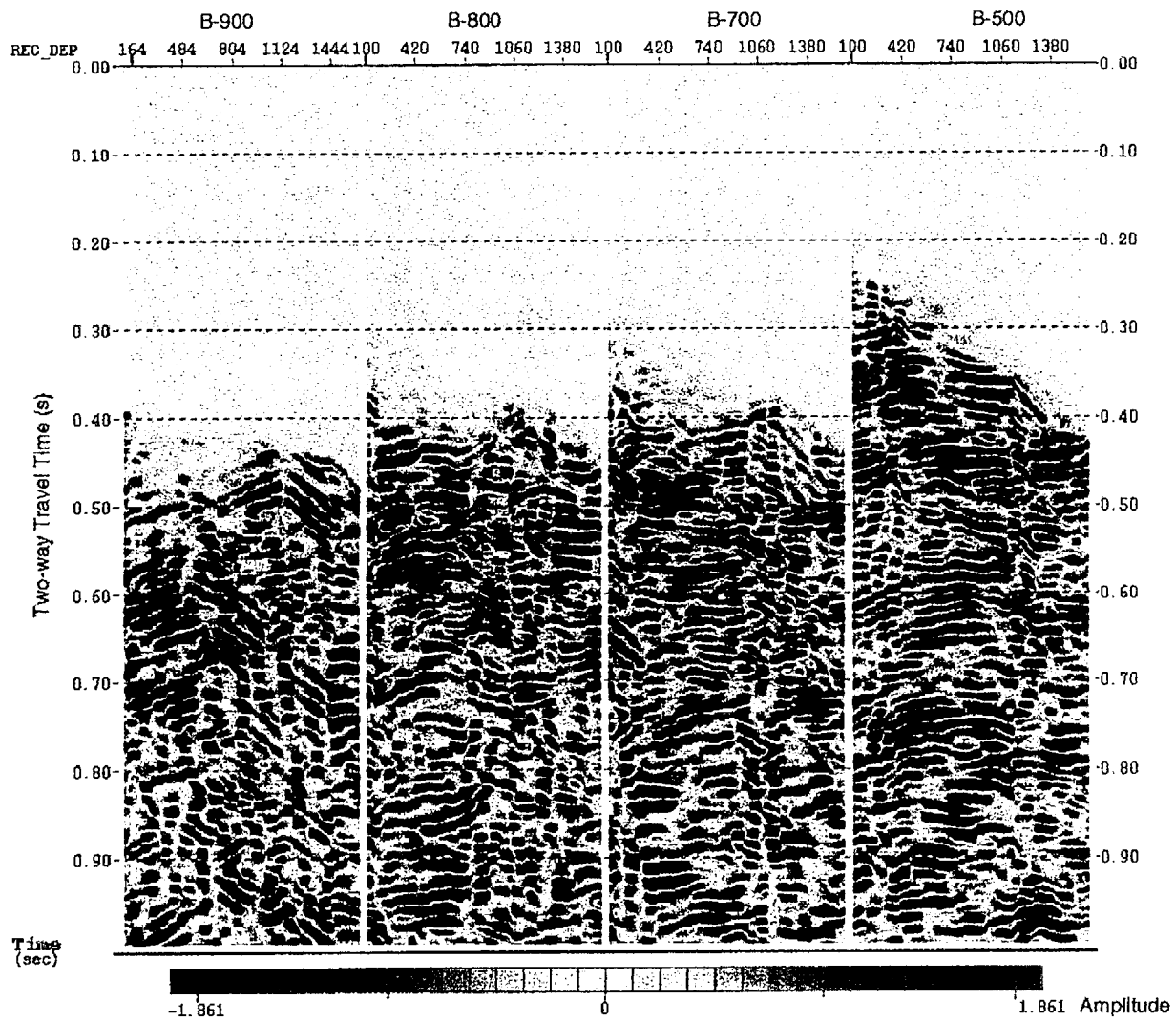


Figure 4b: Same as Figure 4a for source offsets of 500 ft - 900 ft. The data for source offset B-600 is not available.

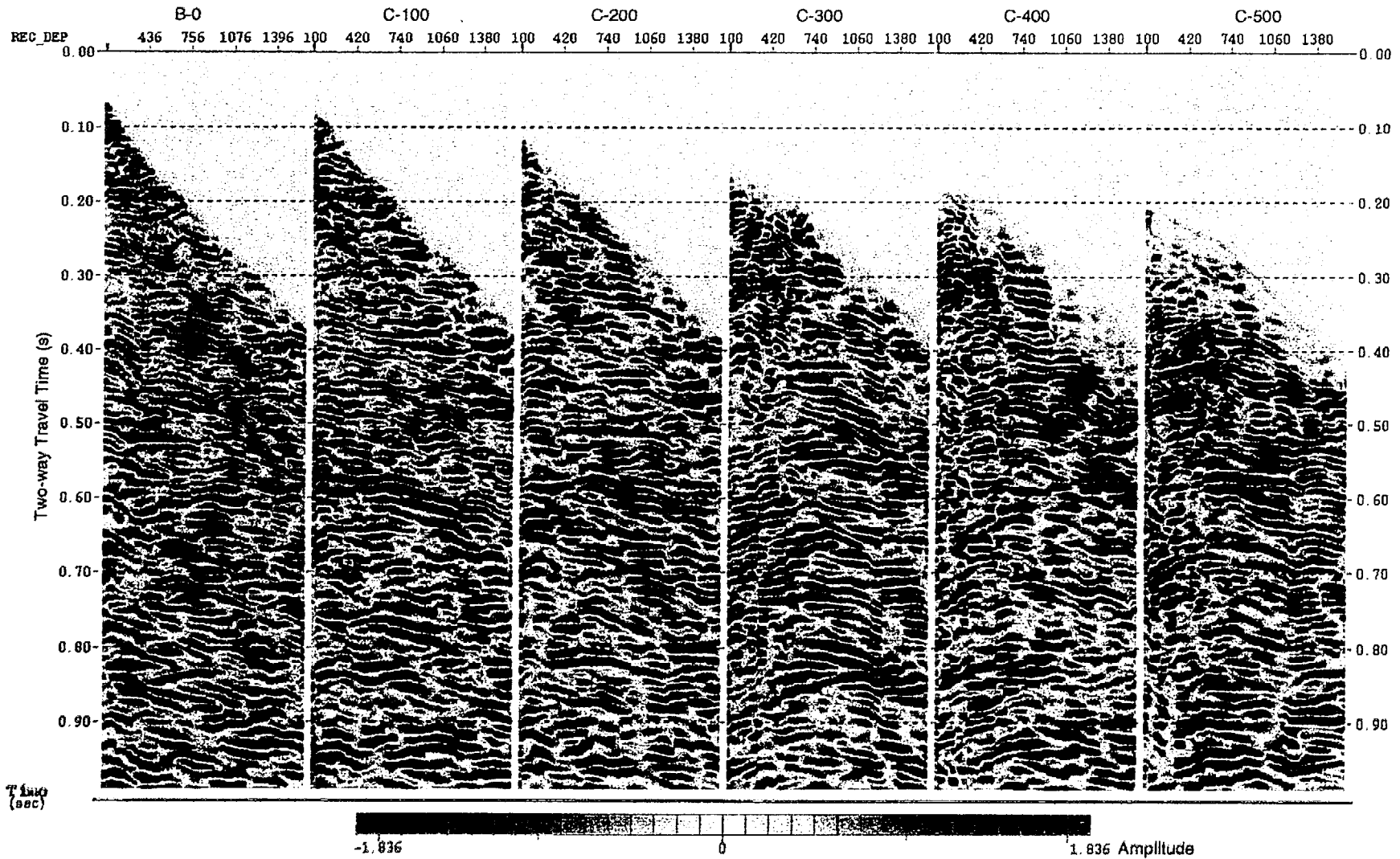


Figure 5a: Same as Figure 4a for source offsets of 0 ft - 500 ft along line C.

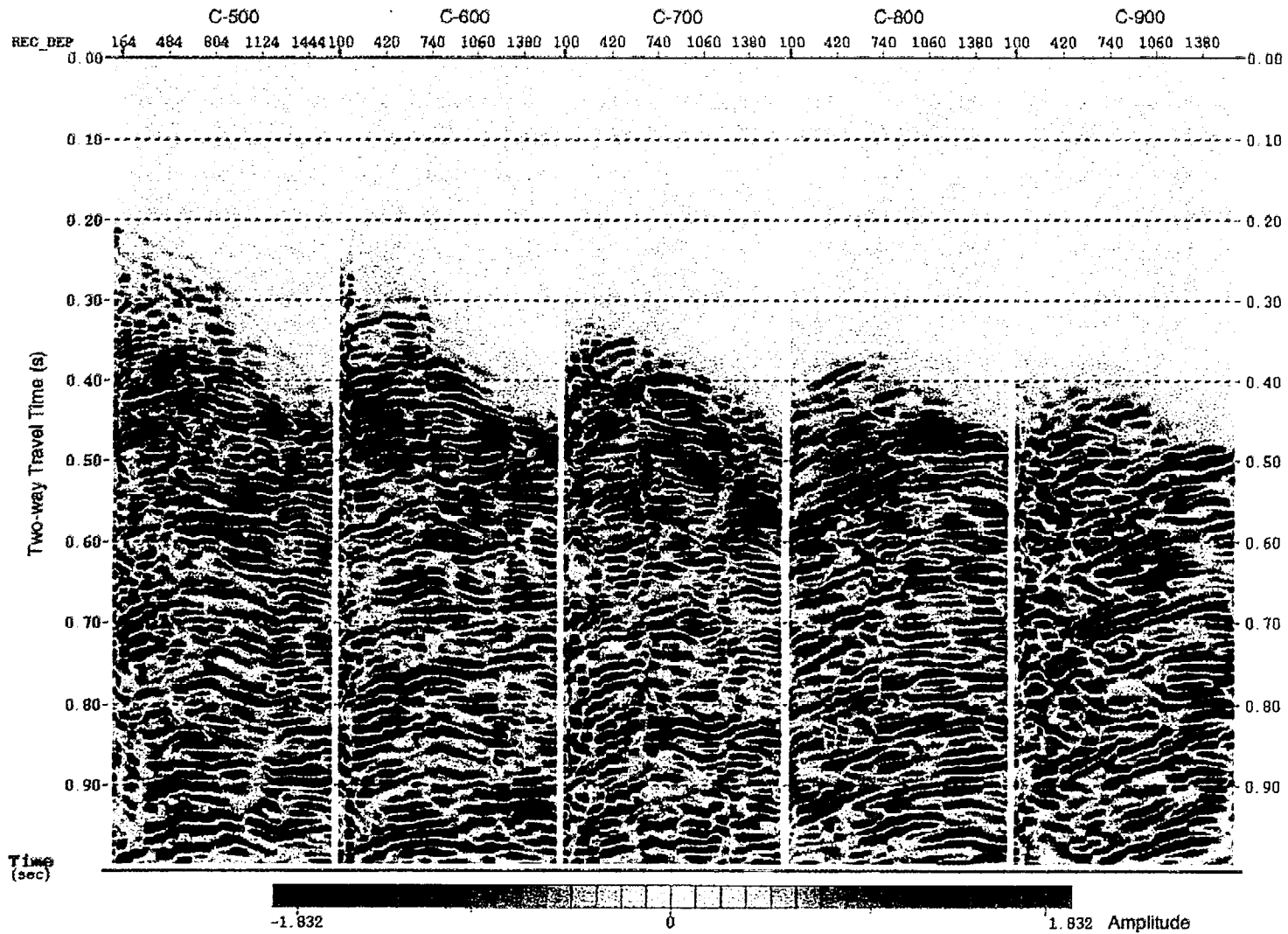


Figure 5b: Same as Figure 4a for source offsets of 500 ft - 900 ft along line C.

### Variation in Velocity Based on First Arrivals

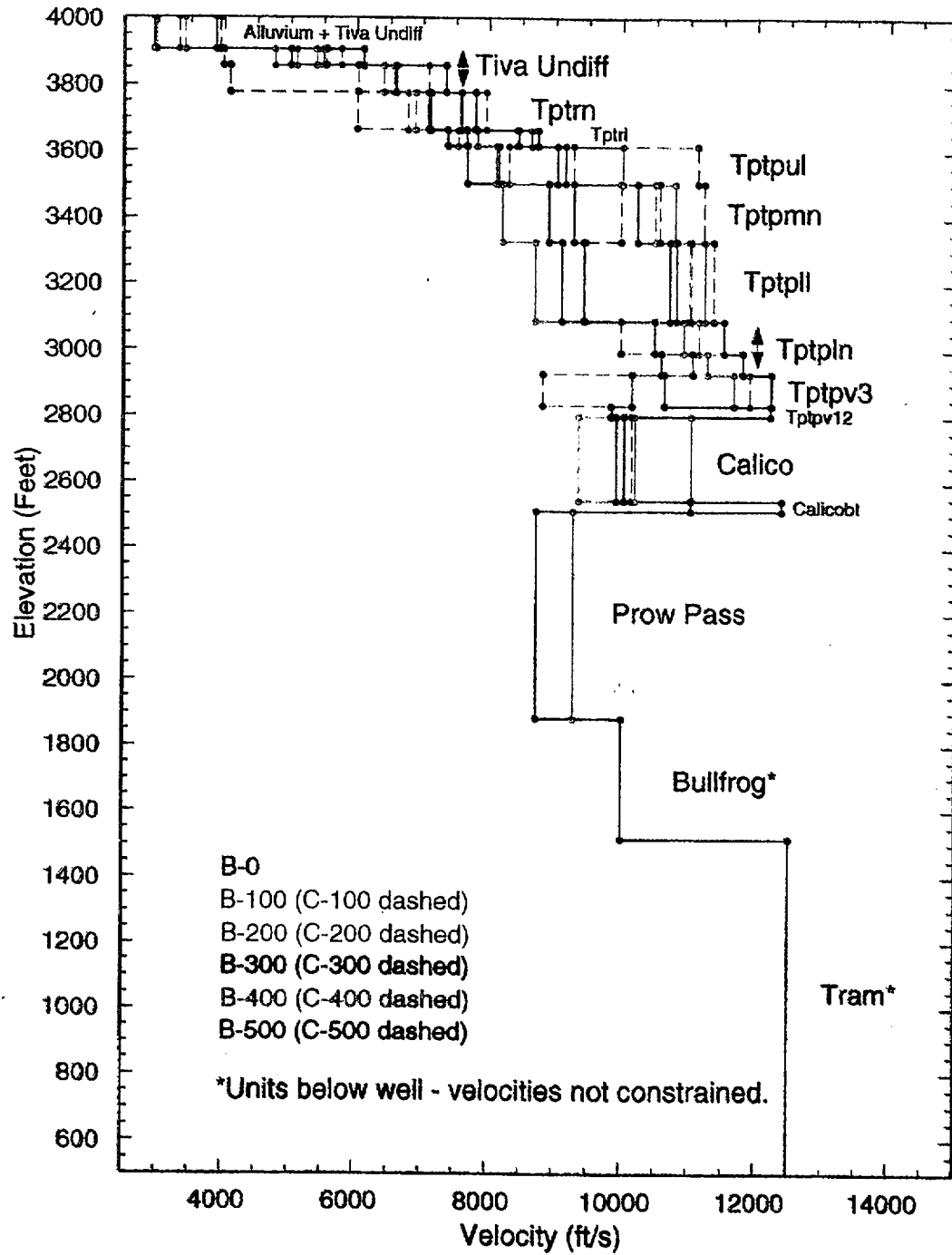


Figure 6: Velocity depth profiles for each source offset along line B and C estimated by fitting the travel times of the down-going waves based on a 6 degree east dipping model. Solid and dashed lines represent the models for line B and C, respectively.

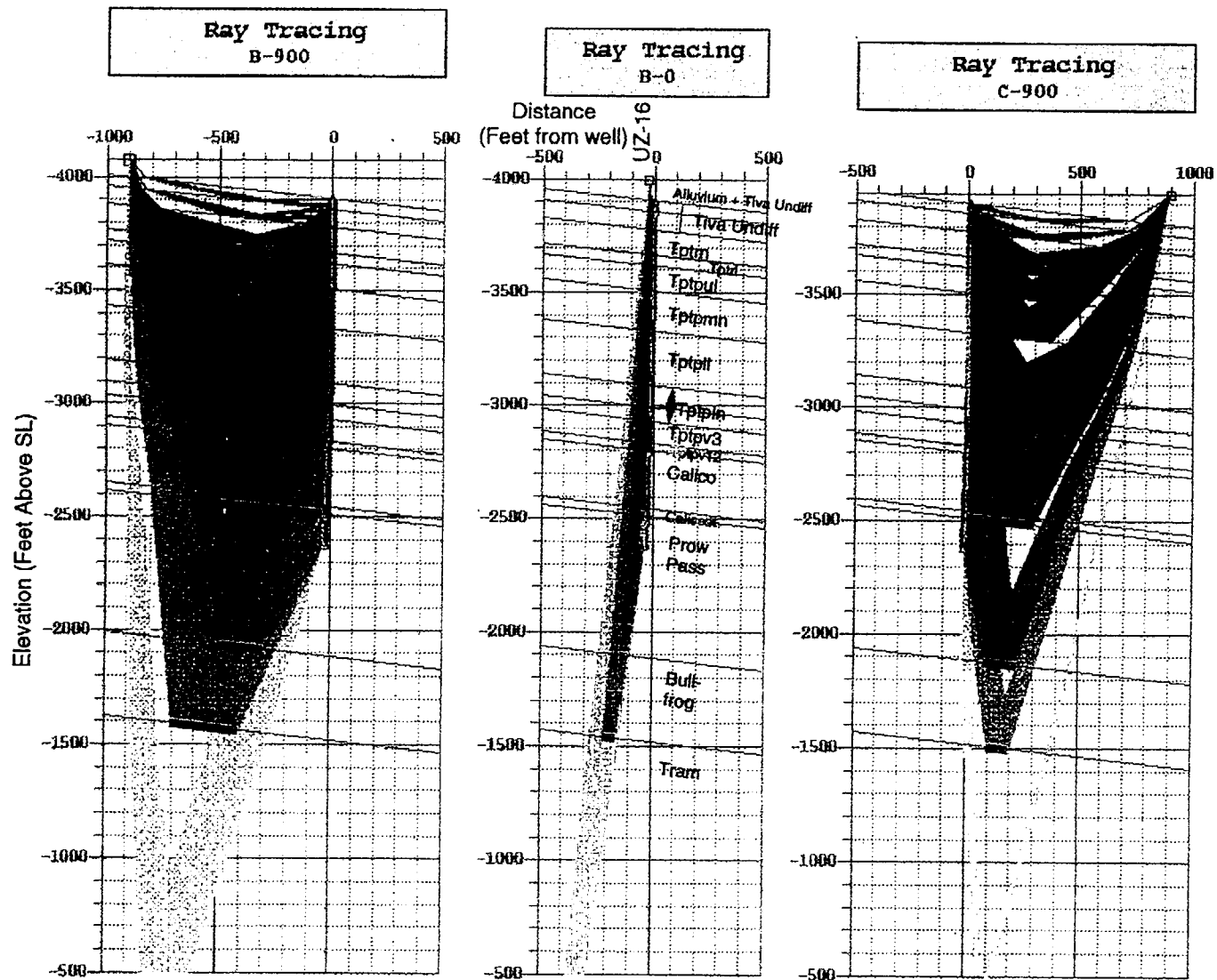


Figure 7: Shown here are the ray paths from the shot (square) to the receivers in the well (small triangles) for the far offsets in this report (B-900 and C-900) and the zero offset shot (B-0). The model dip is 6 degree east. Even though large volumes of rock are being sampled at the large offsets, it is the reflection points (shown as green lines for three deeper events) that determine where the reflections are mapped. The location and width of the reflection points depend on the source/receiver geometry, dip of beds, and the velocity structure. The main effect is from the dipping beds which move the reflection points up-dip and reduce the width of the reflection points for shots down-dip of the well (C-900 compared to B-900).

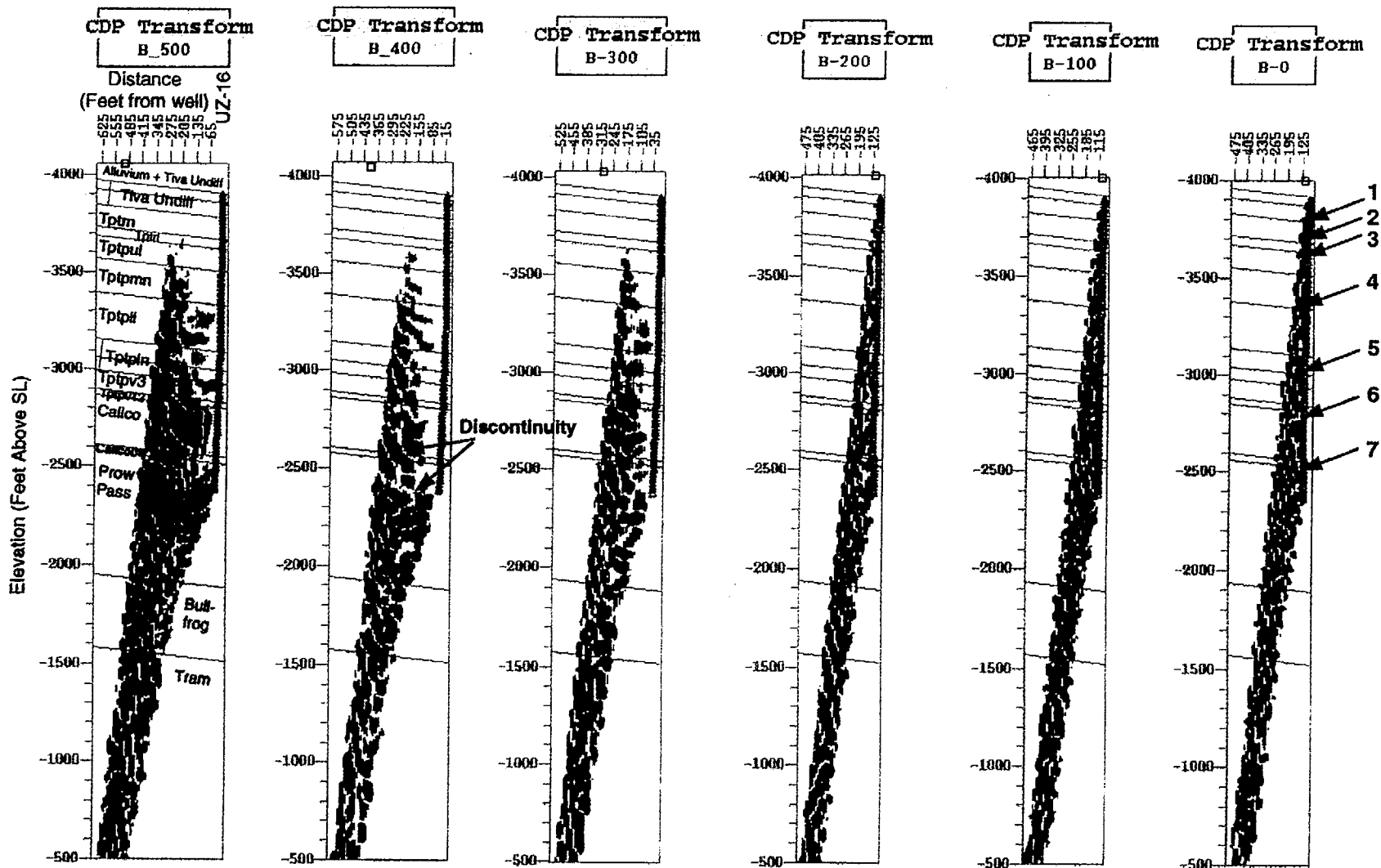


Figure 8a: CDP maps for the first 6 offsets (B0 - B500) of line B (the numbers in the offset titles indicate the distance from the well). The shot and receiver locations are indicated by squares and triangles, respectively. Superimposed on the reflection images is the Yucca Mountain geologic reference model (6 degree east dip). The geologic formations are indicated in the 500 ft offset map.

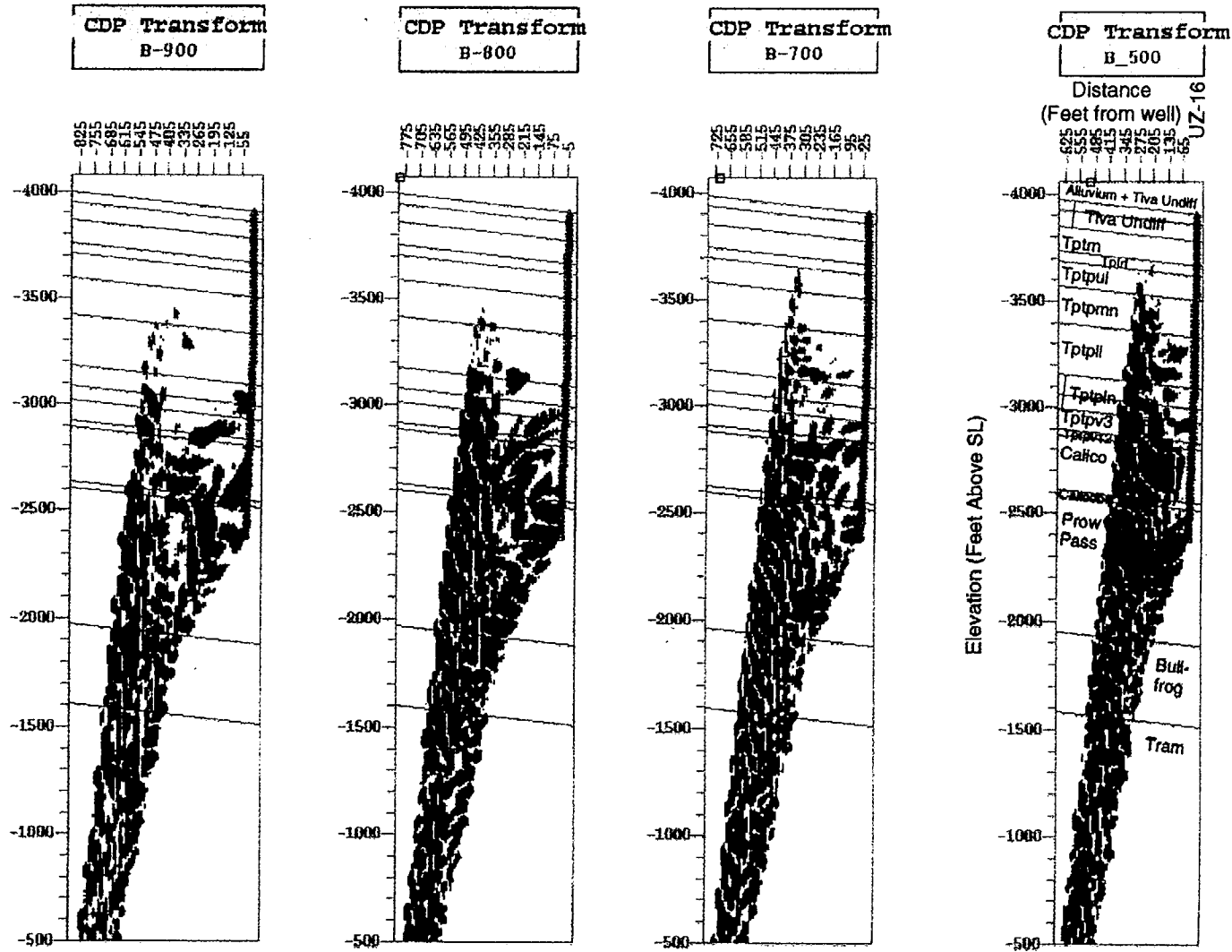


Figure 8b: Same as Figure 8a, for source offsets between 500 ft and 900 ft. The data for the 600 ft source offset are not available.

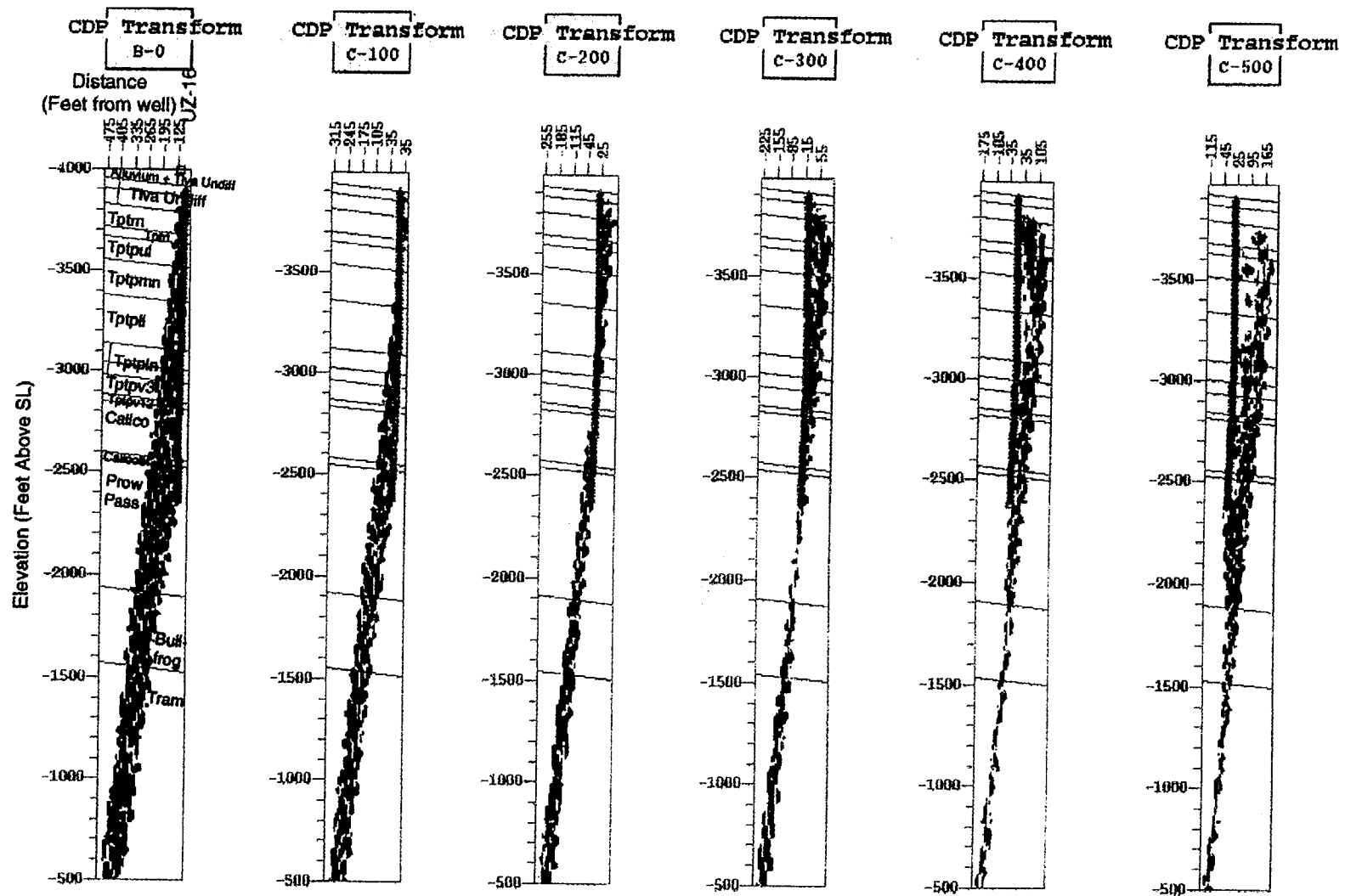


Figure 9a: CDP maps for the first 6 offsets (B0 - C500) of line C..Note the limited extension of the reflection points caused by the up-dip geometry for the shot points along line C.



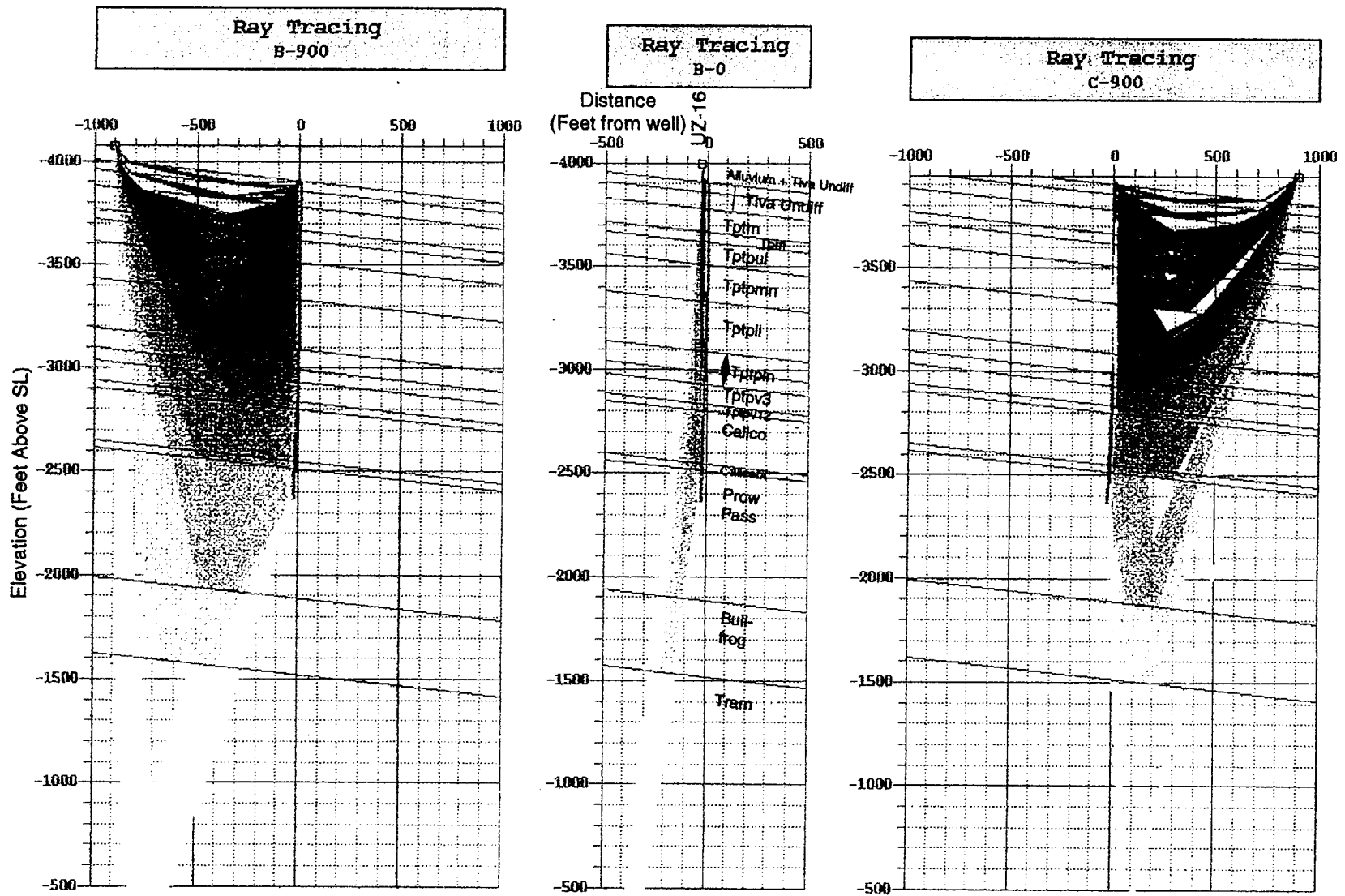


Figure B1: Same as Figure 7 with a dip of 12 degree east.

### Variation in Velocity Based on First Arrivals

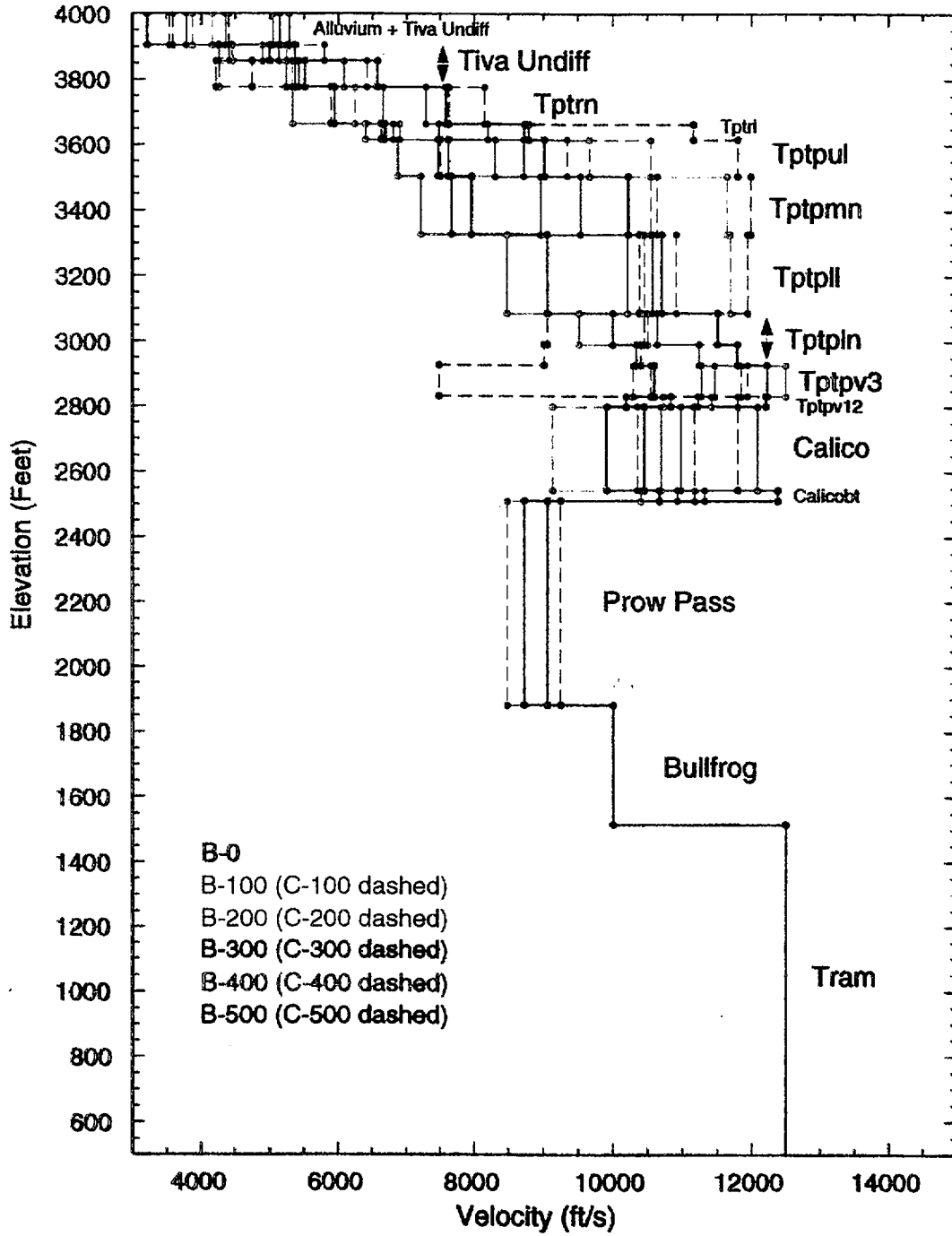


Figure B2: Velocity depth profiles for each source offset along line B and C estimated by fitting the travel times of the down-going waves based on a 12 degree east dipping model. Solid and dashed lines represent the models for line B and C, respectively.

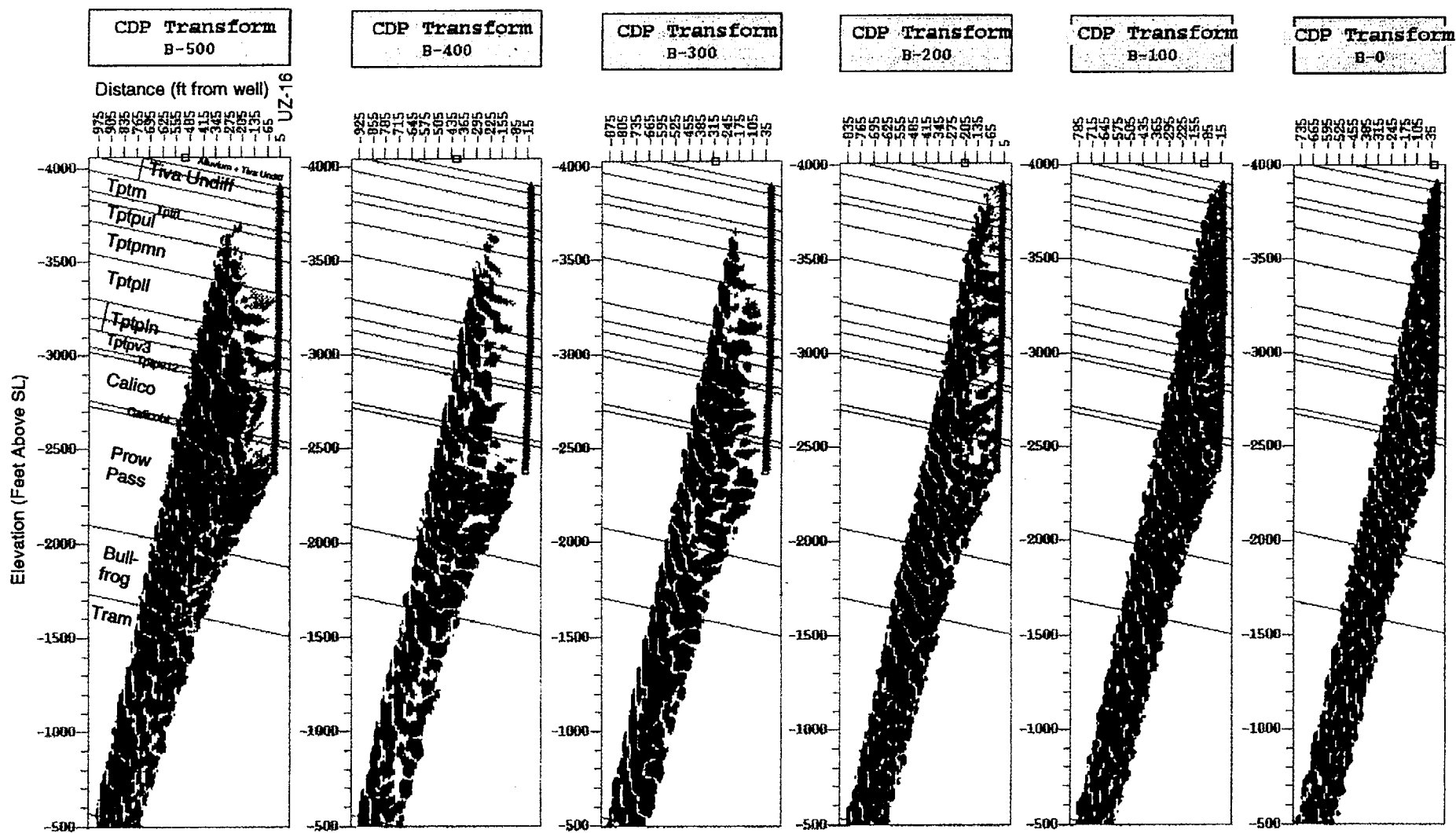


Figure B3a: CDP maps for the first 6 offsets (B0 - B500) of line B. Superimposed on the reflection images is the Yucca Mountain geologic reference model with a changed dip of 12 degree east..

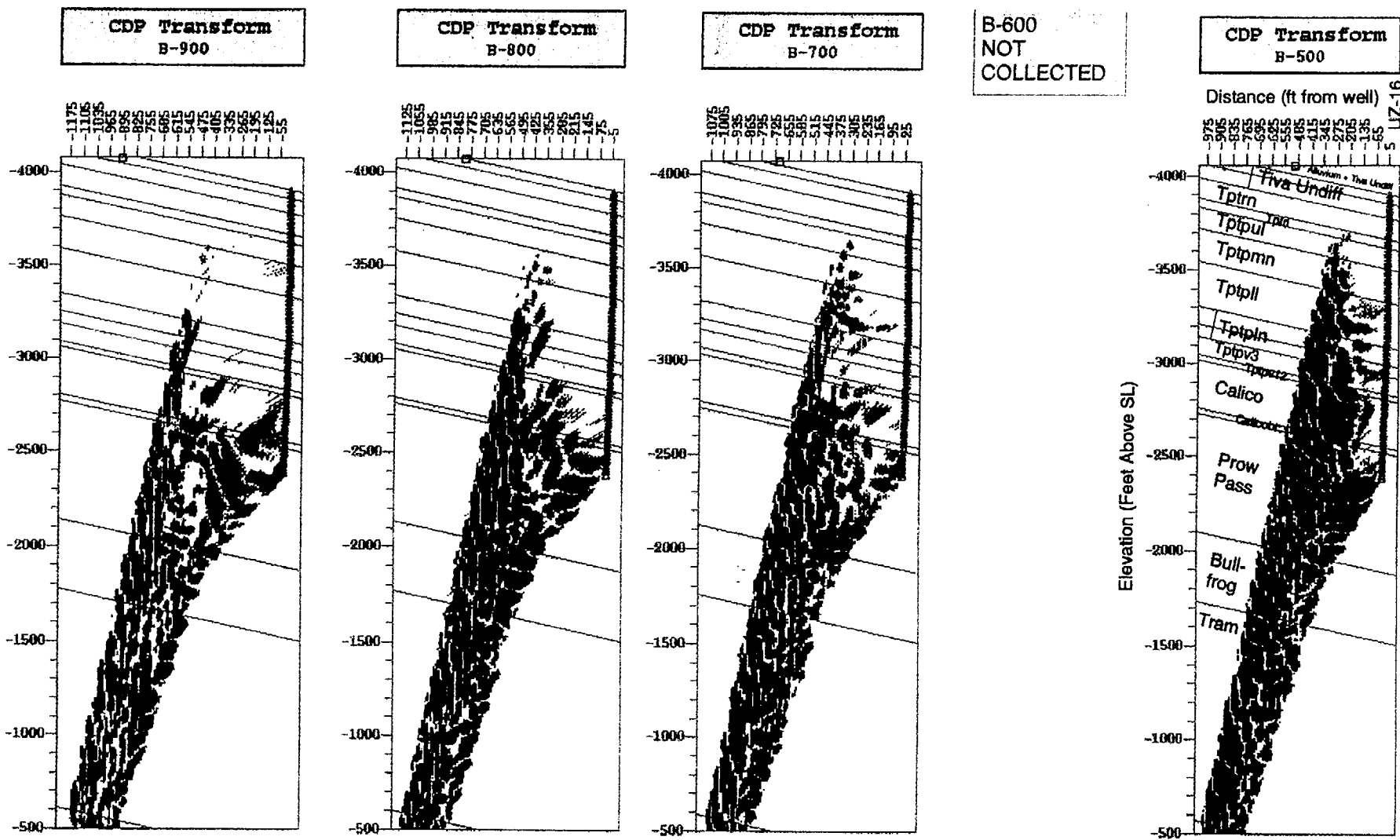


Figure B3b: Same as Figure B3a for the offsets (B500 - B900) of line B.

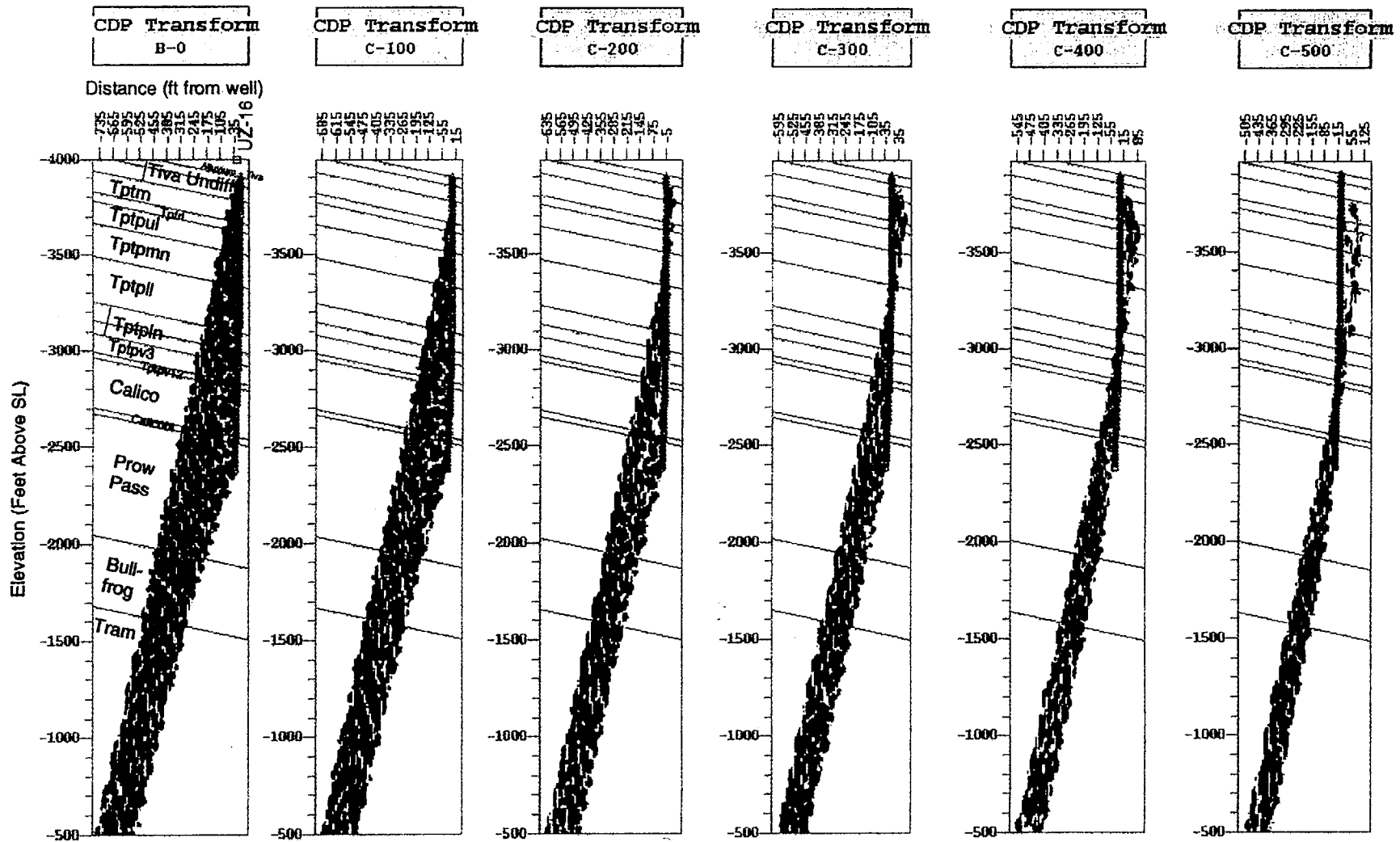


Figure B4a: Same as Figure B3a for the first 6 offsets (B0 - C500) of line C.

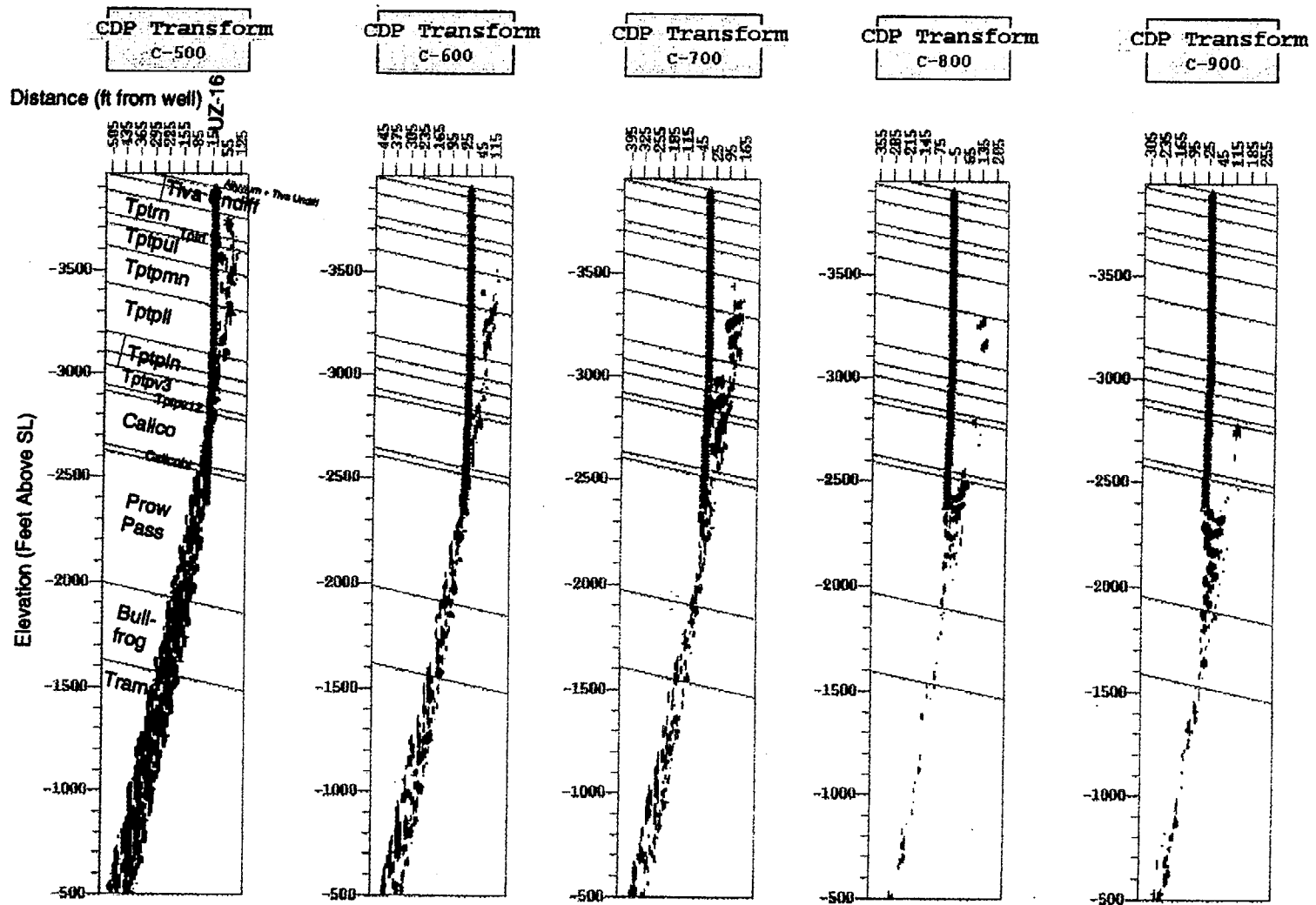


Figure B4b: Same as Figure B3a for the offsets (C500 - C900) of line C.

1/30/78

## DRAFT DISCLAIMER

This contractor document was prepared for the U.S. Department of Energy (DOE), but has not undergone programmatic, policy, or publication review, and is provided for information only. The document provides preliminary information that may change based on new information or analysis, and is not intended for publication or wide distribution; it is a lower level contractor document that may or may not directly contribute to a published DOE report. Although this document has undergone technical reviews at the contractor organization, it has not undergone a DOE policy review. Therefore, the views and opinions of authors expressed do not necessarily state or reflect those of the DOE. However, in the interest of the rapid transfer of information, we are providing this document for your information.